Journal of Hazardous Materials Advances 8 (2022) 100156

Contents lists available at ScienceDirect

Journal of Hazardous Materials Advances

journal homepage: www.elsevier.com/locate/hazadv

Nickel ferrite-based composites and its photocatalytic application – A review

Nagaveni Arumugham[a], Anusuya Mariappan[a,b], Jayanthi Eswaran[a,*], Santhanaraj Daniel[c], Rajakumar Kanthapazham[d,*], Poonkodi Kathirvel[b]

[a] Department of Chemistry, Kongunadu Arts and Science College, G. N Mills post, Coimbatore 641029, Tamilnadu, INDIA
[b] Post Graduate Department of Chemistry, Nallamuthu Gounder Mahalingam College, Palakkad main road, Pollachi 642001, Tamilnadu, INDIA
[c] Department of Chemistry, Loyola College, Chennai 600034, Tamil Nadu, India
[d] Nanotechnology Research & Education Centre, South Ural State University, Chelyabinsk 454080, Russia

ARTICLE INFO

Keywords:
Nickel ferrite-based composites
Photocatalyst
Dye degradation
Pollutants

ABSTRACT

Nickel ferrite-based composites are effectively nominated against an organic pollutant for water remediation. The performance of various nickel ferrite-based composites like binary nickel ferrite-based composites, ternary nickel ferrite-based composites, and carbon nickel ferrite-based composites for the eradication of organic contaminants has been summarized in this review and also briefly discussed the photocatalytic mechanistic pathway to reach the non-harmful products. Obviously, the numerous aspects which support the photocatalytic degradation mechanism to accomplish the maximum removal of pollutants present in water, such as dyes like methylene blue, rhodamine B, methyl orange, congo red, and so on, have also been debated. In addition, the elimination of antibiotics like tetracycline, oxytetracycline, ampicillin, sulfamethoxazole, and organic compounds (phenol) has also been studied using these composites. Overall, this review manuscript provides the reader with information about the recent development of various combinations of nickel ferrite composites and their involvement in the degradation of pollutants as catalysts.

1. Introduction

Life without water is non-viable and becomes a requisite part of all living creatures. On the other hand, rapid industrialization growth and an expanding human population have made the quality of water wrecked. Water bodies like rivers, lakes, ponds, and oceans become contaminated to a greater extent due to the discharge of effluents from dye, food processing, fertilizer, textile, battery, and pharma-based industries (Gusain et al., 2019, Kefeni and Mamba, 2020, Koe, Lee, and Chong, 2019, Mamba et al., 2020, Zheng et al., 2021). These industries release harmful pollutants such as coloured dye compounds, chemical fertilizers, pesticides, organic compounds (phenols, chlorophenols, and nitro-phenols), drugs, heavy metal ions, and infectious micro-organisms. Intake of this contaminated water, either directly or indirectly, will endanger the lives of humans, plants, and animals, and this in turn will eventually affect marine organisms (El-Sayyad et al., 2020). Various remediation methods such as membrane distillation, adsorption, filtration, coagulation, reverse osmosis, electrodialysis, ozonation, oxidation, reduction, and so on have been adopted for the removal of pollutants (Inyinbor, Adekola, and Olatunji, 2016, Oyekanmi et al., 2019, Pangarkar et al., 2014, Pérez-González et al., 2012, Hansima et al., 2021, Rosal et al., 2010, Cui et al., 2020, Wu et al., 2021, Meng et al., 2022, Xu, Li, and Lowry, 2021). Therefore, efforts have been made by the researchers to follow a clean and sustainable approach to destroy the contaminants. Accordingly, photocatalysis is an environmentally friendly process to convert the toxic organic pollutants present in water into non-toxic forms with the influence of a catalyst, and the formation of electron-hole pairs happens in the presence of light. Another added advantage of the following photocatalysis method is that an organic pollutant degrades into small chemical components like CO_2, H_2O, and other chemical species that are not detrimental. The nature of photocatalyst and pollutants, reaction temperature, pH, medium of solvent, source of light used and its intensity, and contact time of the catalyst with organic pollutants are the parameters that show an impact on the efficiency of the photocatalytic degradation process (Gusain et al., 2019). Versatility, stability, consumption of less energy and high efficiency paved the way for the superior quality of the photocatalysis method (Yuan et al., 2021).

On the other hand, photocatalysis can be considered as an advanced oxidation process to degrade an organic contaminant supported by a catalyst and a light source. Researchers have focused on using metal oxide-based materials as photocatalysts like TiO_2 and ZnO, but these

* Corresponding authors.
E-mail addresses: jayakumar.jayanthi@gmail.com (J. Eswaran), kumarkraja84@gmail.com (R. Kanthapazham).

https://doi.org/10.1016/j.hazadv.2022.100156
Received 4 July 2022; Received in revised form 16 August 2022; Accepted 28 August 2022

materials suffer from the weaknesses of broad band gap energies, poor light absorption capacities, and quick recombination of photo-generated electrons and holes without giving their full contribution to the photocatalytic process. In order to avoid this imperfection, they decided to introduce a slight modification to the photocatalytic material. This can be achieved by treating a suitable doping agent with the major photocatalyst material or by forming a nanocomposite by mixing two or three semiconductor materials (Kumar et al., 2016).

In addition to the metal oxide-based material in the photocatalytic application, various spinel ferrite nanoparticles like $CoFe_2O_4$, $CuFe_2O_4$, $ZnFe_2O_4$, $MnFe_2O_4$ and $NiFe_2O_4$ also found their application in the same field of study. It has been well-said that the spinel ferrite nanoparticles were capable of undergoing agglomeration due to the contributions produced by magnetic interactions and Vander Waals forces. Furthermore, these materials produce the dissolution of metal ions in aqueous solutions exposed to greater environmental menaces, which creates their role on the way to limited catalytic application (Qin et al., 2021). Therefore, in order to enhance their catalytic responsibility, the spinel ferrites were coupled with metal oxides like TiO_2 (Nada et al., 2017), Co_3O_4 (Syed et al., 2021), CdO (Janani et al., 2021), polymers (Sandoval et al., 2019), metals (Tsvetkov, Zaharieva, and Milanova, 2020), and carbon-based materials (Bharadwaj et al., 2021). Thus, the aim of this review is to focus on $NiFe_2O_4$-based composites since they have gathered considerable scrutiny due to their reusable and magnetically separable nature (Kefeni and Mamba, 2020). Moreover, we have discussed the $NiFe_2O_4$-based composites and their use in the degradation of organic hazardous waste from the contaminated water environment.

2. Purpose of this review

For the past few decades, the interest in studies based on ferrites and spinel ferrites has been directed more among the scientific community, especially towards the removal of water contaminants. Amongst the several types of ferrites, spinel ferrites have drawn much attention because of their biocompatibility and recoverability. Due to this consideration, the researchers developed an intense interest in writing a review based on spinel ferrites as a photocatalytic material, specifically in degrading organic contaminants. Based on this, the researchers reported reviews on the synthesis, characterization, properties, and applications of spinel ferrites, and some reviews on spinel ferrite nanocomposites in both the fields of adsorption and photocatalytic degradation (Kefeni and Mamba, 2020, Qin et al., 2021, Suresh et al., 2021, Kefeni, Mamba, and Msagati, 2017, Masunga, Kefeni, and Mamba, 2019, Sonu et al., 2019, Park et al., 2019, Amiri, Eskandari, and Salavati-Niasari, 2019, Singh et al., 2019, Narang and Pubby, 2021, Sharifianjazi et al., 2020, Kirankumar and Sumathi, 2020, Masmali, Osman, and Arof, 2021, Mmelesi et al., 2021, Ismael, 2021, SOUFI et al., 2021). To our knowledge, no reported review study has been focused on nickel ferrite-based composites and their photocatalytic application. Herein, we made an attempt to write a review based on the above-mentioned composites on the way to degrade organic pollutants.

3. Nickel ferrite-based composites

Nickel ferrite ($NiFe_2O_4$) is a magnetic ferrite material of inverse spinel structure in which Fe^{3+} ions are placed equally at octahedral and tetrahedral sites whereas Ni^{2+} ions at octahedral sites only (Kefeni et al., 2019, Hezam et al., 2020). Moreover, it has been found with fabulous electrical and physical properties, great chemical stability, excellent saturation magnetization, and a distinctive magnetic structure (Zeynizadeh and Rahmani, 2019, Iftikhar et al., 2019, Online et al., 2016). The role of pristine $NiFe_2O_4$ as a photocatalyst is found to be weaker mainly in the visible light region and also exhibits the quick recombination of photo-induced electron-hole pairs, making an unfavourable performance towards photocatalytic activity. This can be revised by doping $NiFe_2O_4$ with other noble metals, which results in the formation of heterojunction between $NiFe_2O_4$ and semiconductor material. In doing so, the efficiency of photocatalytic degradation of organic contaminants becomes strengthened (Reddy et al., 2020, Gebreslassie et al., 2019, Babu et al., 2020, Rahman et al., 2020). Similarly, when a semiconductor nanomaterial or a carbon-based material merge with $NiFe_2O_4$ to produce $NiFe_2O_4$-based composites, they in turn create some alterations in the surface morphology, potential energy, energy band gap value, charge formation, separation, and distribution, thereby providing a betterment in the photocatalytic activity (Mamba et al., 2020).

The multitalented $NiFe_2O_4$-based nanocomposites were enrolled in various activities such as reduction in which $Bi_2O_2CO_3/NiFe_2O_4$ used to convert 4-nitrophenol into 4-aminophenol (Zarringhadam and Farhadi, 2017), electrocatalyst in which $NiFe_2O_4$/reduced graphene oxide ($NiFe_2O_4$/rGO) used to detect furazolidone which is an antibacterial and an antibiotic drug (Ensafi and Rezaei, 2019), and an elimination process in which $NiFe_2O_4$/carbon sphere eliminated levofloxacin by activating co-catalyst persulfate (Wang et al., 2019). Besides those applications, the most effective and economical way to approach discarding organic pollutants for water remediation depends on adsorption. Accordingly, researchers have prepared numerous $NiFe_2O_4$-based adsorbent as a remedy for water contaminants such as $NiFe_2O_4/MnO_2$ and $NiFe_2O_4$/chitosan to remove lead(II) and fluoride ions, respectively (Xiang et al., 2016, Kumar, Singh, and Singh, 2019). Additionally, $NiFe_2O_4$/graphene oxide ($NiFe_2O_4$/GO) and $NiFe_2O_4$/rGO employed to discard uranium(VI), thorium(IV), arsenic(III) and arsenic(V) by adsorption (Lingamdinne et al., 2016, Online et al., 2016). The $NiFe_2O_4$/hazelnut-shell-based activated carbon was prepared to remove direct red 31 and direct blue 78 dyes from the polluted water through an adsorption process (Livani and Ghorbani, 2017). Table 1 shows the various combination of $NiFe_2O_4$-based composites and the method followed for its preparation, and also its application in numerous fields.

Where MWCNTs - multi-walled carbon nanotubes, PPCOT - poly(pyrrole-co-O-toluidine), C-SWCNTs - cross-linked single-walled carbon nanotubes, PAMPS - polymer of (2-acrylamide-2-methyl propane sulfonic acid), CNTs - carbon nanotubes and PAMA - poly acrylonitrile co maleic anhydride

From the details given in Table 1, we can see the majority of $NiFe_2O_4$-based composites find their application in the field of adsorption. But unfortunately, the downside of the adsorption process is the creation of secondary waste products, which further become an environmental concern. Therefore, for the ecological betterment, the path for remediation to degrade the contaminants moved towards the photocatalytic process, in which the formation of only non-harmful products after the degradation.

3.1. Synthesis methods and parameters

The factors such as size, shape, and properties of nanomaterials are highly controlled by the preparation procedure, which in turn affects the efficiency of catalytic activity (Ismael, 2021, SOUFI et al., 2021) Generally, synthesizing nanomaterials can be classified into two ways: top-down and bottom-up approaches. In the top-down method, the large-sized chemical substances are crushed to form tiny nanomaterials, whereas in the bottom-up method, the smaller ions undergo reaction and then combine together to form a nanomaterial (Sonu et al., 2019, Mmelesi et al., 2021). Mechanical milling and laser ablation are the commonly used top-down methods, whereas, co-precipitation, hydrothermal, solvothermal, sol-gel, microemulsion, thermal decomposition, microwave-assisted, sono-chemical and electrochemical methods comes under the category of bottom-up methods (Sonu et al., 2019, Mmelesi et al., 2021, Ismael, 2021, SOUFI et al., 2021). Among these two methods, the bottom-up method is widely followed to synthesize nanomaterials, and besides, each preparation method has its own qualities, which are unavoidable (Ismael, 2021, SOUFI et al., 2021).

Table 1
Types of $NiFe_2O_4$-based composites, method adopted for preparation and application

S. No	$NiFe_2O_4$-based nanocomposite	Method of preparation	Application	Ref no:
1.	$NiFe_2O_4$/polythiophene	Co-precipitation and chemical oxidative polymerization of thiophene	Janus green B and Fuchsin basic dyes removal by adsorption	(Hussain and Siddiqui, 2020)
2.	GO/$NiFe_2O_4$/layered double hydroxide	One-pot hydrothermal method	Congo red (CR), Methyl orange (MO) and Cr^{6+} (VI) ions removal by adsorption	(Zheng et al., 2019)
3.	Poly (vinylidene fluoride-co-hexafluoropropylene)/$NiFe_2O_4$	Chemical co-precipitation and electrospinning method	Energy harvest	(Ponnamma et al., 2019)
4.	$NiFe_2O_4$ nanocrystals encapsulated by graphene	Hydrothermal and chemical reduction method	Lithium-ion batteries	(Tong et al., 2017)
5.	GO/$NiFe_2O_4$ /polypyrrole	Hummer's method, sol-gel auto-combustion method and pyrrole's polymerization	Storage of energy	(Ahmad et al., 2020)
6.	$NiFe_2O_4$/rGO	Co-precipitation and sonochemical method	Direct red 81 and basic blue 41 dyes removal by adsorption	(Bazgir et al., 2019)
7.	3-D graphene/chitosan/$NiFe_2O_4$	One-pot hydrothermal method	Removal of Pb ions through adsorption method	(Nasiri, Arsalani and Panahian, 2018)
8.	$NiFe_2O_4$/carbon	Polymerization process	Cancer phototherapy	(Gorgizadeh, Azarpira and Sattarahmady, 2018)
9.	$NiFe_2O_4$/MWCNTs	Sol-gel auto-combustion method followed by ultra-sonication	Cr^{6+} ions removal from electroplating discharge	(Verma and Balomajumder, 2020)
10.	Ternary PPCOT/$NiFe_2O_4$/C-SWCNT	Oxidative chemical polymerization	Electrochemical sensor to detect Fe^{3+} ions	(Katowah et al., 2020)
11.	$BaFe_{12}O_{19}$/$NiFe_2O_4$	Co-precipitation method	-	(Thirupathy et al., 2020)
12.	Alginate grafted PAMPS/$NiFe_2O_4$	Oxidative-free radical grafted polymerization	Methylene blue (MB) dye and Cu^{2+} ions removal by adsorption	(Al and Tohamy, 2020)
13.	$LaFeO_3$-$NiFe_2O_4$	Egg-white method	-	Muthu, Lakshminarasimhan and Perumal, 2017
14.	$NiFe_2O_4$/rGO	Co-precipitation and solvothermal method	Microwave absorption technology	(Kumar et al., 2020)
15.	$NiFe_2O_4$@SiO_2/MWCNT	Thermal decomposition, Stöber process and ultra-sonication	Electromagnetic wave absorption technology	(Xiong et al., 2019)
16.	$NiFe_2O_4$/rGO	Hydrothermal method	Supercapacitor applications	Bagher and Salarizadeh, 2020
17.	Glutathione-functionalized $NiFe_2O_4$/GO	Hummer's method and ultra-sonication	Removal of Hg^{2+}, Cu^{2+}, Pb^{2+} ions by adsorption process	(Khorshidi, 2020)
18.	Glutaraldehyde-grafted chitosan@$NiFe_2O_4$	Modified solvothermal method and ultra-sonication	MO and CR dyes removal by adsorption	Moghaddam et al., 2018
19.	$NiFe_2O_4$/graphene	Solvothermal method	Hydrogen evolution reaction	(Nivetha et al., 2017)
20.	rGO/MWCNTs/$NiFe_2O_4$	Ultra-sonication and hydrothermal process	Electromagnetic wave absorption technology	(Wu et al., 2019)
21.	$NiFe_2O_4$/carbon	Calcination	Sonodynamic cancer therapy	(Gorgizadeh et al., 2019)
22.	$NiFe_2O_4$/rGO	Self-combustion process	-	(Boychuk et al., 2019)
23.	$NiFe_2O_4$/CNTs	One-step hydrothermal method	Pseudocapacitor and energy storage applications	Kumar et al., 2017
24.	$NiFe_2O_4$/activated carbon	Co-precipitation and hydrothermal method	-	Livani, Ghorbani and Mehdipour, 2018
25.	Polyrhodanine/$NiFe_2O_4$	Co-precipitation and chemical polymerization technique	Antibacterial activity	Lashkenari, Ghorbani and Naghibi, 2019
26.	$NiFe_2O_4$-N doped mesoporous carbon	Thermal method	Elimination of Hg^{2+} ions from contaminated water using adsorption method	(Naushad et al., 2017)
27.	Poly(m-phenylenediamine)/ $NiFe_2O_4$	Oxidative polymerization	-	Muthusamy, Arunkumar and Kannapiran, 2017
28.	Polyrhodanine/$NiFe_2O_4$	Oxidative chemical polymerization process	Catalytic role in oxidation of hydrazine reaction	(Soleimani and Shahrokhi, 2018)
29.	$NiFe_2O_4$/rGO	Hydrothermal method	-	(Boychuk et al., 2018)
30.	$NiFe_2O_4$/rGO	Solvothermal process	Role of electrocatalyst in hydrogen evolution reaction	Mukherjee et al., 2018
31.	$NiFe_2O_4$/activated carbon	Hydrothermal process	Elimination of ibuprofen and ketoprofen from water through adsorption process	(Foletto and Dotto, 2019)
32.	$NiFe_2O_4$/titanium oxide	-	Removal of Cr^{4+} ions from polluted water	(Shekari et al., 2017)
33.	Gum ghatti-*cl*-poly(acrylamide)/$NiFe_2O_4$	Free radical polymerization method	To eliminate ciprofloxacin hydrochloride by adsorption	(Gor and Dave, 2019)
34.	$NiFe_2O_4$/PAMA/Ag-TiO_2	Three-step method procedure	Antibacterial activity	(Allafchian et al., 2015)
35.	$NiFe_2O_4$/polyaniline	Hydrothermal and chemical oxidative polymerization	Alizarin red S removal by adsorption	Liang, He and Zhang, 2017

$FeNi_3$ ($NiFe_2O_4$)/chitosan/BiOI nanocomposites have been prepared based on co-precipitation and sol-gel methodologies. Based on the SEM and TEM images of $NiFe_2O_4$ and BiOI, the morphology of both the materials showed spherical and sheet-like structures as shown in Fig. 1. Further, BiOI along with chitosan forms an outer coating of $NiFe_2O_4$/chitosan/BiOI, which may come into direct contact with the aqueous dye solution. Thus, the synthesized nanocomposites were highly porous, amorphous, and rough in nature, which supported the degradation pathway towards success (Sadat et al., 2021). The HRTEM image of $NiFe_2O_4$/SnO_2 quantum dots (SQD) showed the deposition of

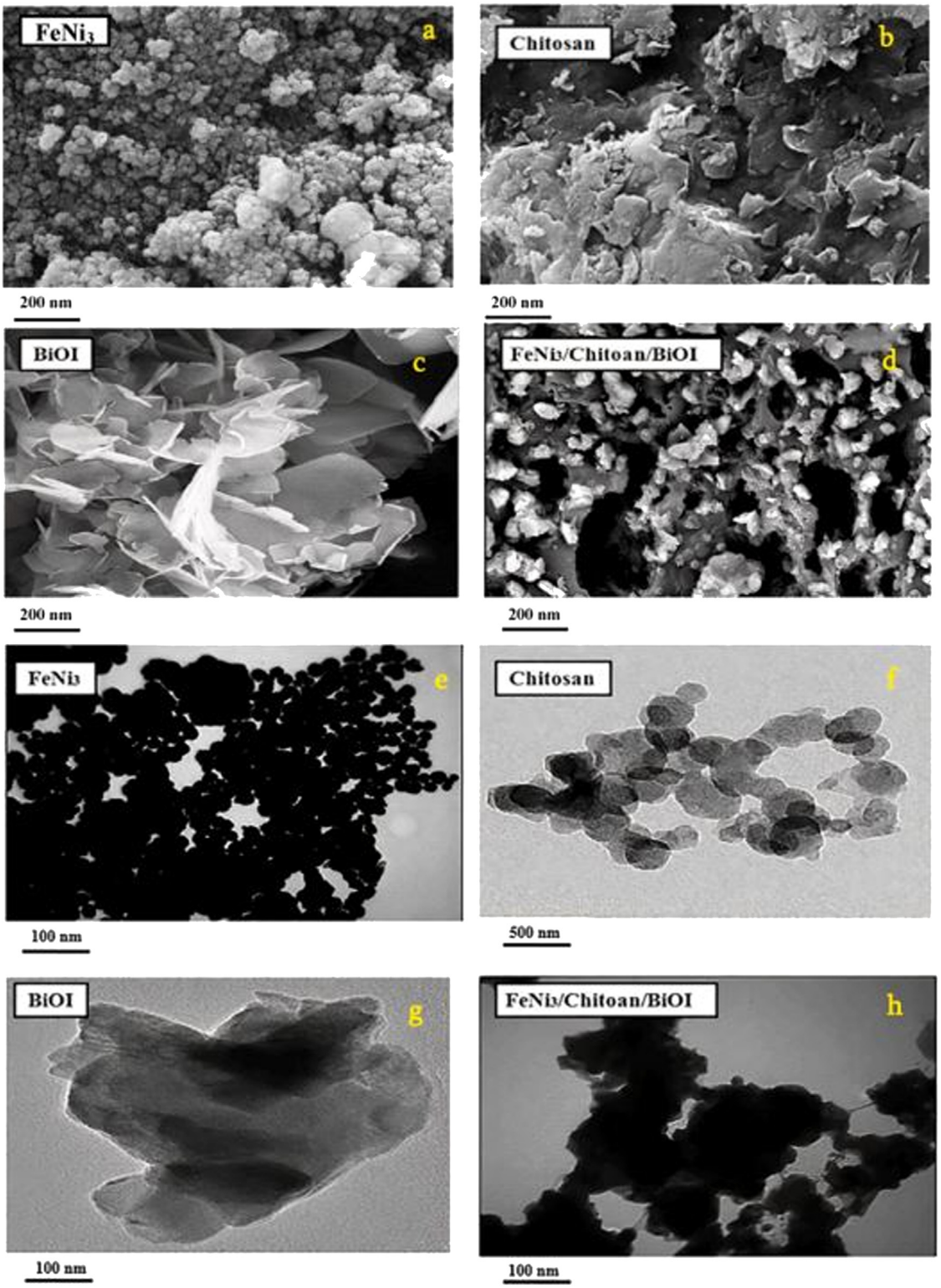

Fig. 1. FESEM (a-d) and TEM (e-h) images of $FeNi_3$, chitosan, BiOI, and $FeNi_3$/chitosan/ BiOI. Reproduced with permission from ref (Sadat et al., 2021), copyright 2021, Elsevier.

SQD on the $NiFe_2O_4$ surface and the lattice fringe patterns had spacings of 0.246 nm and 0.339 nm, corresponding to (311) and (110) planes respectively of $NiFe_2O_4$ and SnO_2, as shown in Fig. 2. This aspect confirmed the heterojunction development between the two materials and was further verified by a selected area electron diffraction (SAED) pattern, which became a favourable route for photocatalytic activity (Babu et al., 2020).

The high purity and porous nature of $ZnS/NiFe_2O_4$ nanocomposites showed their efficiency in dye degradation under sunlight conditions. Further, the surface area value of these composites was found to be

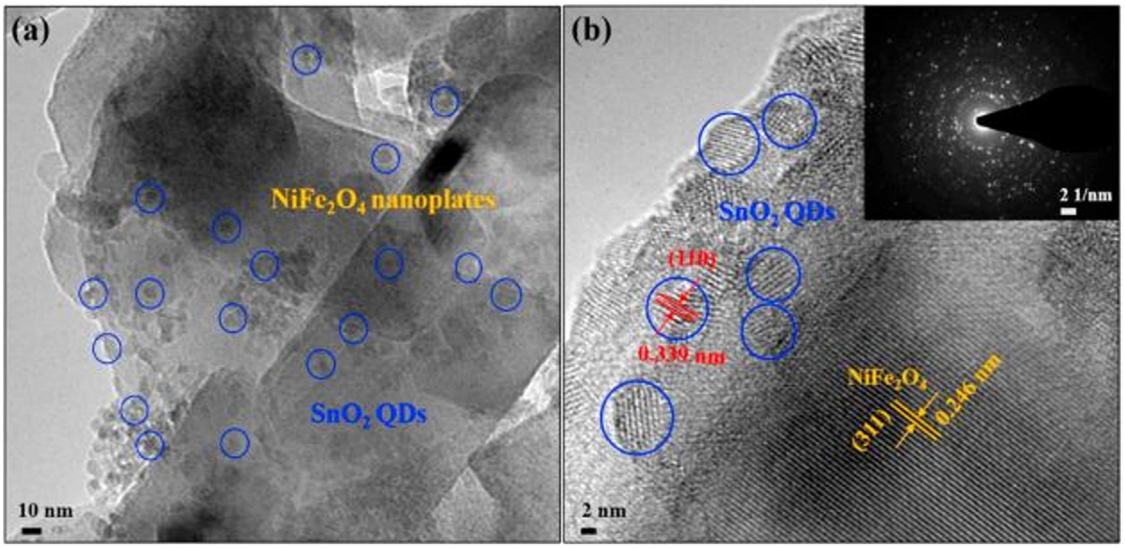

Fig. 2. (a) HRTEM image and (b) lattice fringe pattern of the $NiFe_2O_4$/SQD nanocomposite (NFS-10) in the HRTEM image. Reproduced with permission from ref (Babu et al., 2020), copyright 2020, Elsevier.

44.72 m^2/g, obtained from the study of BET analysis. Thus, the higher surface area and homogeneous distribution of the particles favoured the degradation pathway (Dharmaraja et al., 2021). The metal nitrates ($Fe(NO_3)_3.9H_2O$ and $Bi(NO_3)_3.5H_2O$), metal chloride ($NiCl_2.6H_2O$) and KBr were used in a facile hydrothermal method to prepare various content ratios of BiOBr/$NiFe_2O_4$ composites. Under the basic pH condition, the mixtures were poured into a Teflon-lined autoclave at 140 °C for 15 h. After cooling to room temperature, the particles were purified using water and further dried at 50 °C. This method of treating composites had a significant impact on enhancing the photocatalytic activity (Li et al., 2017).

3.2. Binary/ternary nickel ferrite-based composites towards dye degradation

Composite materials are combination of two or more non-identical materials which display the properties different from the original parent materials (Dutt et al., 2020). Moreover, a composite can gain the qualities of each individual material, which makes it highly advantageous to take part in the role of applications (Suresh et al., 2021). Thus, in spite of the good stability, biocompatibility, and low band gap energy values of nickel ferrites, they show a faster recombination rate of charge carriers, which shows less attention to the degradation process. With this aspect, researchers created binary/ternary nickel ferrite-based composites as an alternative, which can generate more free radicals, retard the recombination rate, and show a good synergistic effect. Thus, a binary composite of $NiFe_2O_4/TiO_2$, used as an effective photocatalyst, degraded turquoise blue 21 dye in the presence of sunlight. Based on the results obtained, the $NiFe_2O_4/TiO_2$ binary composite showed the highest achievement in the degradation of dye (Shah, Joshi, and Shah, 2022). Visible light enhanced photocatalytic degradation of meropenem has been achieved using $NiFe_2O_4$/metal organic framework (MOF)-808. The best degradation efficiency was produced when using a 1:2 mass ratio of $NiFe_2O_4$:MOF-808 and pH 6 (Khosroshahi, Bakhtian, and Safarifard, 2022).

Through a hydrothermal method, $NiFe_2O_4$ nanoparticles were prepared, which were then coated onto cellulose nanofibres (CNF) made from waste biomass (pine needles) to give cellulose-$NiFe_2O_4$ nanocomposites (CNF-$NiFe_2O_4$). Additionally, silanization of cellulose-$NiFe_2O_4$ nanocomposites (SCNF-$NiFe_2O_4$) was also prepared through the silanization process. Then, those two cellulose nanocomposites were taken as photocatalysts to degrade remazol black dye under an Xe lamp. Various ratios of CNF to $NiFe_2O_4$ (5:1, 2.5:1 and 1.5:1) were prepared and the results showed that CNF-$NiFe_2O_4$ (2.5:1) composites ratio provided good degradation efficiency, which was attributed to the synergistic effect formed between cellulose nanofibres and $NiFe_2O_4$ compared to other ratios. Due to the larger surface area and improved thermal stability of the photocatalyst, the SCNF-$NiFe_2O_4$ (2.5:1) composite ratio demonstrated 98.6 % removal efficiency using a catalyst amount of 50 mg (Gupta et al., 2017).

A two-step simple process was used to prepare $NiFe_2O_4/Bi_{24}O_{31}Br_{10}$ nanocomposites and study their photocatalytic performance towards the degradation of crystal violet dye from aqueous solution under visible light radiation. When bare $NiFe_2O_4$, $Bi_{24}O_{31}Br_{10}$, 10 % $NiFe_2O_4/Bi_{24}O_{31}Br_{10}$, 20 % $NiFe_2O_4/Bi_{24}O_{31}Br_{10}$ and 30 % $NiFe_2O_4/Bi_{24}O_{31}Br_{10}$ were compared, the 20 % $NiFe_2O_4/Bi_{24}O_{31}Br_{10}$ nanocomposites with outstanding stability and great photocorrosion resistance show the best removal efficiency. Photoluminescence (PL) spectra of 20 % $NiFe_2O_4/Bi_{24}O_{31}Br_{10}$ clearly emphasized the lower chance of recombination ability of charge carriers because of lower PL intensity. Also, due to the absorption of visible light by $NiFe_2O_4/Bi_{24}O_{31}Br_{10}$ nanocomposites, the emergence of holes in VB and electrons in CB of both $NiFe_2O_4$ and $Bi_{24}O_{31}Br_{10}$ has been achieved. The potential energy difference created the transfer of electrons and holes from CB of $NiFe_2O_4$ to CB of $Bi_{24}O_{31}Br_{10}$ and VB of $Bi_{24}O_{31}Br_{10}$ to VB of $NiFe_2O_4$, respectively. The involvement of electrons with O_2 produced superoxide radicals ($O_2^{\bullet-}$) radicals, which in turn led to generate ȮH radicals by reaction with H^+ ions. Those ȮH radicals involved in the decomposition of crystal violet dye into CO_2 and H_2O molecules. On the other hand, the performance of holes dealt directly with the crystal violet dye molecules towards degradation (He et al., 2019).

Immobilization of glucose oxidase (GOx) on $NiFe_2O_4$/Tannin ($NiFe_2O_4$/T) to produce $NiFe_2O_4$/T/GOx and the formation and degradation mechanism of indigo carmine dye were illustrated in Fig. 3. The photocatalytic activities of $NiFe_2O_4$, $NiFe_2O_4$/T and $NiFe_2O_4$/T/GOx were performed on indigo carmine dye for decolorization in the presence of UV radiation and by performing the Fenton process. Complete degradation of dye has been attained after 12 hours of contact time with $NiFe_2O_4$/T/GOx nanocomposite as a catalyst in the Fenton process. In that process, the formation of H_2O_2 was allocated to the enzymatic performance of GOx and successively produced active ȮH radicals due to the reaction between H_2O_2 and Fe^{2+}/Fe^{3+}.

Finally, dye degradation was accomplished on account of the reaction between ȮH radicals and dye molecules to yield the products of

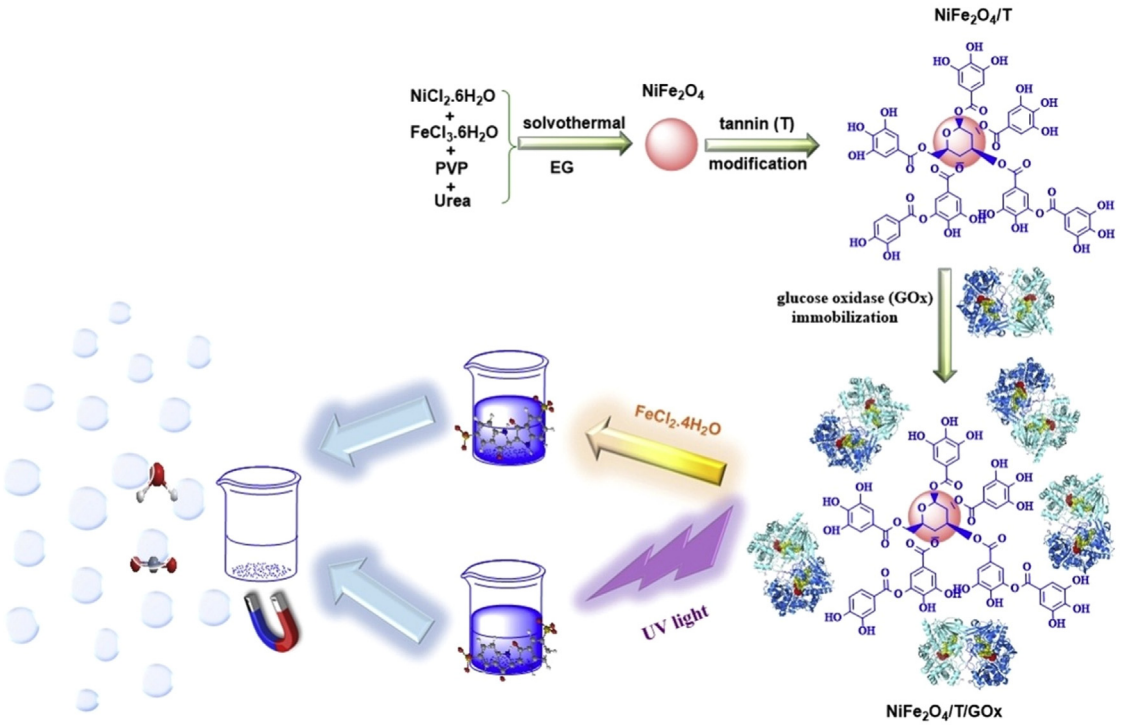

Fig. 3. Formation and degradation mechanism of indigo carmine dye using $NiFe_2O_4$/T/GOx. Reproduced with permission from ref (Atacan et al., 2019), copyright 2019, Elsevier.

CO_2, H_2O, and mineral acids. Whereas, decolorization under UV light displayed higher-level performance compared to the above process since the mechanism involved was both enzymatic and photocatalytic for $NiFe_2O_4$/T/GOx nanocomposites. First of all, enzymatic performance has taken place similar to the Fenton process to create ȮH radicals. After that, the charge transfer mechanism to generate hydroperoxyl and $O_2^{\cdot-}$ radicals, which then reacted with dye molecules, caused serious devastation of indigo carmine dyes (Atacan et al., 2019).

3.3. Comparative study of dye degradation using binary/ternary nickel ferrite-based composites

Nickel ferrite-graphitic carbon nitride ($NiFe_2O_4$-g-C_3N_4) used as a photocatalyst to degrade MB and Rhodamine B (RB) dyes under solar and LED irradiation (Fig. 4). Results showed that the degrading performance of both the dyes was higher for solar light compared to LED. This was attributed to higher absorption of $NiFe_2O_4$ in the NIR region and the formation of a defect band, and also heterojunction development between $NiFe_2O_4$ and g-C_3N_4. Further, the addition of H_2O_2 to enhance the catalytic process produced hydroxyl radicals, which facilitated the degradation process more efficiently. The proposed mechanism for dye degradation can be illustrated as follows. As a result, the conduction band (CB) energy value of g-C_3N_4 (-1.13 eV) was discovered to be more negative than the CB energy of $NiFe_2O_4$ (0.24 eV), implying that photo-induced electrons were transferred from the former to the latter. On the other hand, shifting of positive holes occurred in the opposite direction owing to the high valence band (VB) potential of $NiFe_2O_4$. Furthermore, because of the more negative CB energy compared to the standard reduction potential, those electrons in the CB of g-C_3N_4 were involved in the process of producing $O_2^{\cdot-}$ by reaction with O_2 and also converted H_2O into H_2O_2. Furthermore, the involvement of $O_2^{\cdot-}$ radicals with H_2O_2 causes the formation of ȮH. After those processes, the destruction of dye molecules leads to the origination of non-harmful chemical compounds (Palanivel et al., 2019).

Photocatalytic activity of $NiFe_2O_4$-NiO nanocomposites prepared by the precipitation method was performed to remove organic azo dyes, namely acid blue 92, acid brown 14, acid black 1, and acid violet from the waste water under UV radiation. Decolorization of all the dyes happened through the formation of active species such as $O_2^{\cdot-}$ and ȮH radicals, which were produced under the effect of UV light and photo-generated charge carriers. Among all the dyes, a higher percentage of removal had been accomplished for acid blue 92 by following the same reaction conditions, and the final outcome formed after the degradation of dyes was CO_2, H_2O, and non-toxic chemical species (Saffarzadeh, Nabiyouni, and Ghanbari, 2016). Paul A and Dhar S. S. prepared $MnMoO_4$/$NiFe_2O_4$ nanocomposites through co-precipitation and hydrothermal methods using corresponding metal salts, and PEG 400 was used as a stabilizing agent. Photocatalytic activity of $MnMoO_4$/$NiFe_2O_4$ nanocomposites was performed against MB, RB, methyl violet, and basic fuchsin dyes under visible light. Compared to bare $NiFe_2O_4$ and $MnMoO_4$, the degrading efficiency of all dyes increased to a greater extent using $MnMoO_4$/$NiFe_2O_4$ nanocomposites as photocatalyst, due to the exchange of electrons between $NiFe_2O_4$ and $MnMoO_4$, and also on account of delayed recombination of electron-hole pairs. Usage of scavengers like isopropanol, benzoquinone, and ammonium oxalate was found to reduce the efficiency of degradation (Paul and Dhar, 2019).

Magnetic $NiFe_2O_4$@ZnO nanocomposites applied as a photocatalyst to degrade the pollutants such as direct blue 129 and reactive blue 21 dyes from the waste water under visible light conditions. Results showed that by varying the initial dye concentration and keeping photocatalyst dosage constant, the removal efficiency was found to be highest for a lower dye concentration. The reason was that, at higher concentrations, the dye molecules act as a blockade and, consequently, the penetration of light into the surface of the catalyst seemed to be very difficult (Moradi, Taghavi, and Ali, 2018).

Anionic dye degradation occurred to a greater extent than cationic dye degradation in the presence of UV and visible radiation using

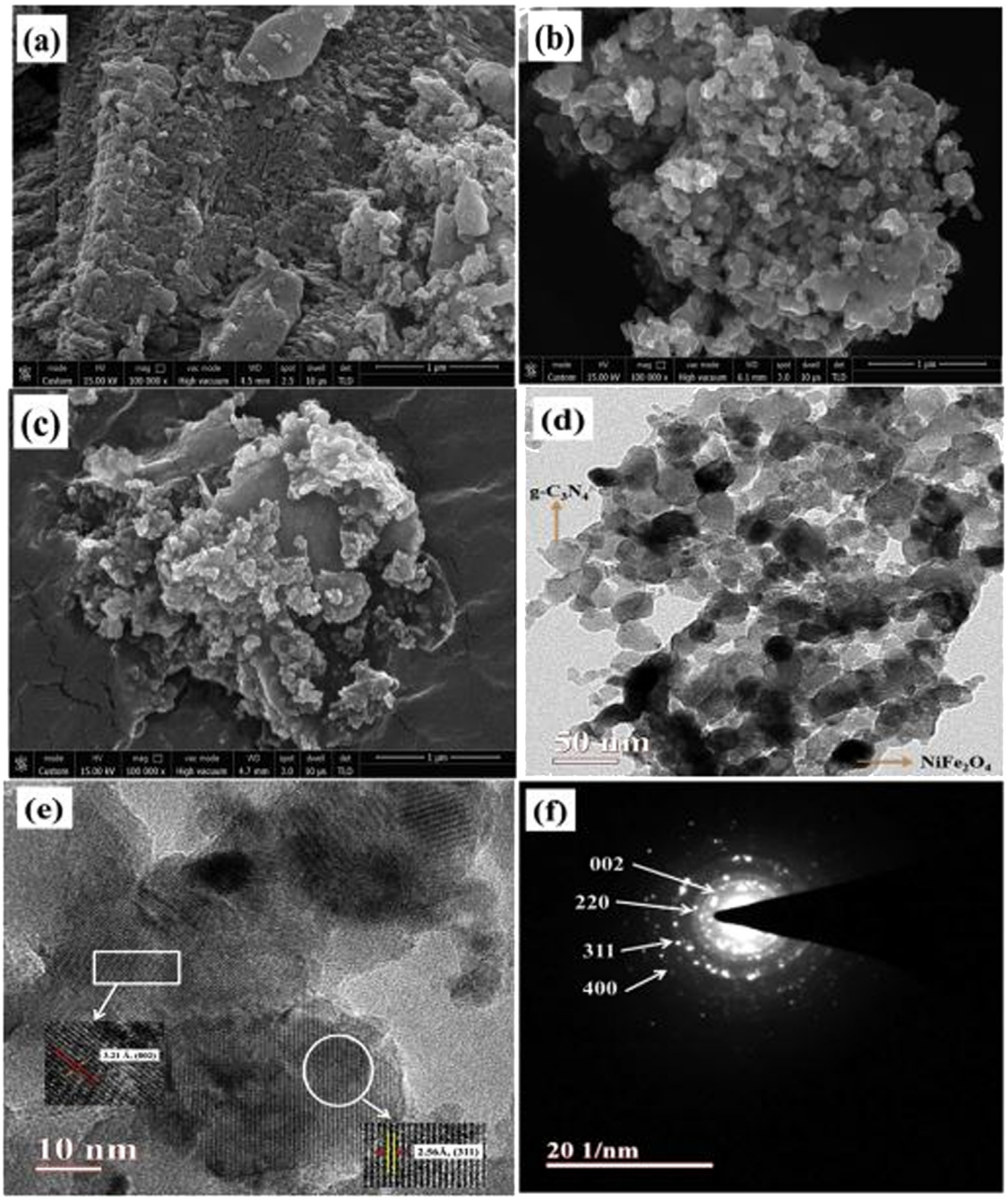

Fig. 4. FESEM images of (a) g-C_3N_4, (b) $NiFe_2O_4$, (c) $NiFe_2O_4$-g-C_3N_4; (d) TEM image of $NiFe_2O_4$-g-C_3N_4, (e) HRTEM image of $NiFe_2O_4$-g-C_3N_4, (f) SAED pattern of $NiFe_2O_4$-g-C_3N_4. Reproduced with permission from ref (Palanivel et al., 2019), copyright 2019, Elsevier.

$NiFe_2O_4/SiO_2$/Au photocatalyst which had been prepared by the following sonochemical method (Fig. 5). In addition, maltose and Crataegus pentagyna were used as capping and reducing agents, respectively, during the synthesis. Because of the presence of more oxygen atoms and positive charges on the dye, erythrosine, an anionic dye, demonstrated the highest removal efficiency under UV illumination when compared to cationic dyes such as RB and MB. The mechanisms involved in the degradation process were the adsorption of dye molecules onto the catalytic surface followed by charge transfer to create ȮH and $O_2^{\bullet-}$ radicals. The destruction of organic dyes achieved due to the involvement of those active radicals with the organic moiety of dye molecules led to the formation of non-hazardous products. The photocatalytic performance of $NiFe_2O_4/SiO_2$/Au towards dye degradation could withstand even up to seven cycles with a minute loss in weight, thereby proving as a promising candidate to enrol in the process of dye decolorization (Mohammad et al., 2020).

4. Photocatalytic degradation of organic pollutants

Photocatalytic degradation of organic pollutants uses a photocatalyst, which is an active material that increases the rate of the chemical reaction without causing any damage to the substance. They are photocatalysts that are both homogeneous and heterogeneous. In a homogeneous photocatalyst, as the name indicates, the reactant as well as the catalyst are in the same phase, whereas in a heterogeneous photocatalyst, the phases are different for the reactant and the catalyst. The

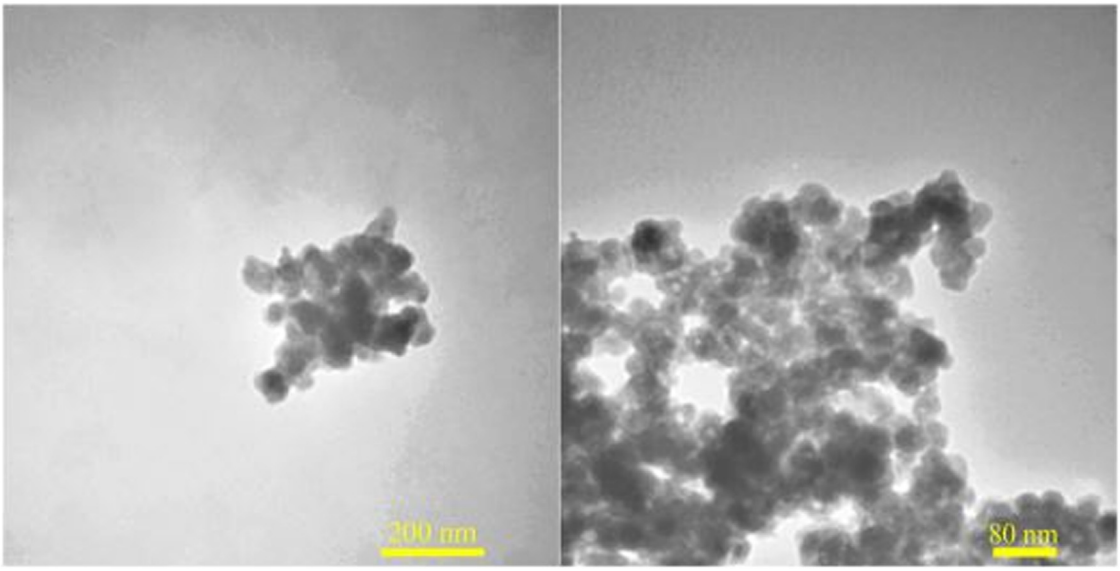

Fig. 5. TEM images of as-obtained NiFe/Si/Au nanocatalyst. Reproduced with permission from ref (Mohammad et al., 2020), copyright 2020, John Wiley and Sons.

latter photocatalyst has additional advantages compared to the former in terms of stability and recyclability to accomplish the complete degradation of organic pollutants (Hassan and Jalil, 2022). As per a statistical report, more than 100,000 commercial dyes are available in the world, with a yearly production of 7×10^5 tonnes of dyes (Xiao et al., 2021, Brillas and Martínez-Huitle, 2015). Taking this feature into consideration, our researchers have developed various photocatalytic materials to eradicate the dye-stuffs from the environment. Among these, $NiFe_2O_4$-based composites, a heterogeneous catalyst mainly involved in this elimination process. The intention and requirement for the removal of particular dyes from the contaminated water have been described under the corresponding headings. Moreover, these composites played their role in degrading phenol and antibiotics.

4.1. Photocatalytic degradation of methylene blue dye

A water-soluble cationic dye, MB is utilized largely in the industries of cotton, textiles, and leather. As a result, when effluents are discharged into the water environment, they cause problems for both marine and human life. The presence of MB in water generates a delay in sunlight transmission, which leads to a reduction in the photosynthesis process of aquatic plants. Furthermore, inhalation causes nausea, vomiting, and diarrhoea in humans, as well as irritation of the eyes and gastrointestinal tract (Jawad et al., 2018, Jawad, Ngoh, and Radzun, 2018, Jawad et al., 2017). Thus, the abolition of toxic MB dye from polluted water bodies is a needed one for environmental protection.

A two-step method has been followed to synthesize $NiFe_2O_4$/MWCNTs/ZnO nanocomposites and the same has been used as a catalyst to degrade MB dye under sunlight conditions. At higher pH 11.55, decolorization of MB dye increased due to the presence of more hydroxide ions compared to lower pH values (3 and 6.66) by following the same reaction conditions. Adsorption and photocatalytic reaction were used to degrade MB dye molecules from an aqueous solution. Initially, stirring causes MB dye molecules to become adsorbed on the surface of the nanocomposites. Furthermore, when exposed to solar radiation, positive holes were produced in the VB of $NiFe_2O_4$ and ZnO, while photo-excited electrons were produced in the CB. Due to the more negative CB potential of $NiFe_2O_4$ compared to ZnO, transfer of electrons occurred from $NiFe_2O_4$ to ZnO and then to MWCNTs through the $NiFe_2O_4$/ZnO interface. Consequently, electrons and holes reacted with O_2 and H_2O to form $O_2^{\cdot-}$ and ȮH radicals respectively. Further reaction of those active species with adsorbed MB dye molecules gave rise to non-detrimental chemical products. The photochemical stability of prepared nanocomposites was maintained well for five cycles (Hezam, Nur, and Mustafa, 2020). To degrade MB dye from the contaminated water, which is a textile pollutant, Surabhi Kamal et al. used BCN/$NiFe_2O_4$ nanocomposites as a catalyst in the presence of visible light irradiation. Unlike pristine BCN and $NiFe_2O_4$, BCN/$NiFe_2O_4$ nanocomposites showed a higher removal efficiency of 98 % in 80 min. This happened due to the lower band gap energy value of BCN/$NiFe_2O_4$ (2.05 eV) over the pure BCN (2.65 eV) and $NiFe_2O_4$ (2.38 eV) from UV-DRS studies as shown in Fig. 6. During the adsorption of visible light by nanocomposites, that could promote the higher production of electron-hole pairs. In this way, the recombination rate of charge carriers became reduced and favoured the enhanced photo-degradation activity (Kamal et al., 2019).

To study the decolorization of MB dye solution under visible light, the catalysts used were Cu_2O, $NiFe_2O_4$, $NiFe_2O_4$@AIMCM-41, and $NiFe_2O_4$@AIMCM-41-Cu_2O, in which AIMCM-41 was a mesoporous material. Among these four catalysts, $NiFe_2O_4$@AIMCM-41-Cu_2O showed 90 % removal efficiency at pH 9 and 60 min of contact time with the dye solution. To begin with, the larger surface area of AIMCM-41 allowed MB dye molecules to quickly adsorb to its surface. Thereafter, AIMCM-41 contained Al atoms in its moiety, which could act as a mediator to transfer the photo-excited negative electrons from the CB of Cu_2O to the CB of AIMCM-41. Then, those electrons were involved in the reduction process to convert Fe^{3+} to Fe^{2+}. Similarly, electrons reacted with H_2O_2 to form ȮH radicals and its anions, which further reacted with MB dye to form the degradation products (Sohrabnezhad and Rezaeimanesh, 2017).

$BiVO_4$ nanoparticles were coated with $NiFe_2O_4$ nanoparticles, a ternary semiconductor material, to produce $BiVO_4$/$NiFe_2O_4$ nanocomposites. Photocatalytic activities were tested using $NiFe_2O_4$, $BiVO_4$ and $BiVO_4$/$NiFe_2O_4$ against MB dye solution in the presence of natural and collected sunlight radiation. The degrading action of MB dye was studied over natural and collected sunlight using $BiVO_4$/$NiFe_2O_4$ nanocomposites as a catalyst. In the presence of collected sunlight, the catalyst showed the highest removal percentage of 98 % in 30 min compared to natural sunlight, which degraded only 39 % According to them, under collected sunlight, the production of photo-induced charge carriers would be greater, and this in turn resisted the recombination rate and thereby led to the improved oxidation-reduction process. During this process, $O_2^{\cdot-}$, ȮH, and its anions were formed, which then reacted with MB dye molecules to produce decomposed products such as CO_2, H_2O,

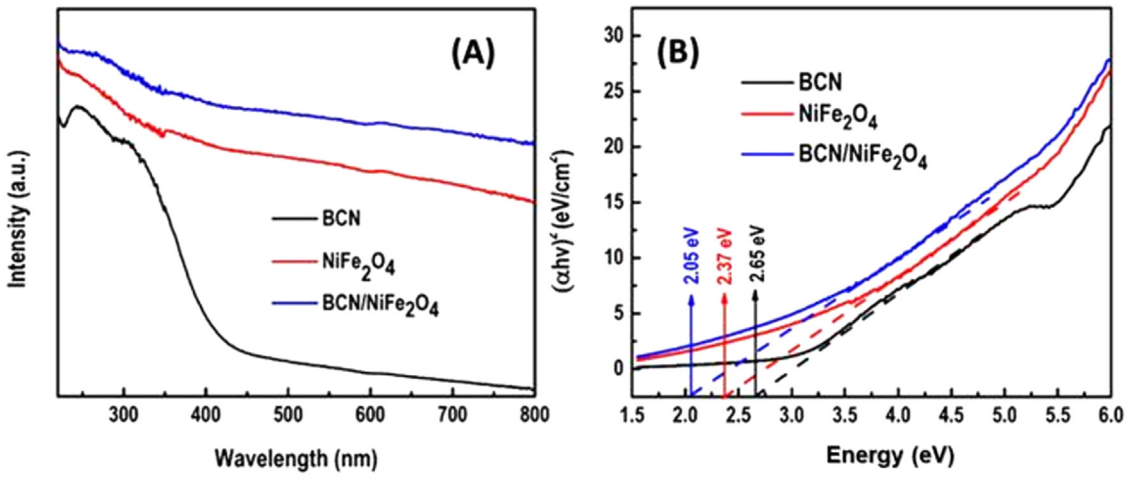

Fig. 6. UV-DRS of BCN, $NiFe_2O_4$ and BCN/$NiFe_2O_4$ nanocomposite (A), the indirect band gap of as-prepared BCN, $NiFe_2O_4$ and BCN/$NiFe_2O_4$ nanocomposite (B). Reproduced with permission from ref (Kamal et al., 2019), copyright 2019, Elsevier.

and non-toxic chemical species. Jianxing Liang et al. followed the ball-milling process to prepare $NiFe_2O_4$-rGO nanocomposites and used them as a photocatalyst to degrade MB dye solution for water remediation under visible light conditions. They found that with increased graphene oxide content in the $NiFe_2O_4$-rGO catalyst, the degradation rate of MB also increased, because rGO has more adsorption sites due to its large surface area, and, additionally, π-π stacking formed between MB dye molecules and rGO. While using graphene oxide content of 0.35, almost 99.1 % degradation has been achieved. Following that, increasing the graphene oxide content resulted in a decrease in degradation, which was attributed to the low $NiFe_2O_4$ content. This clearly indicated that $NiFe_2O_4$ nanoparticles also had an effect on the photocatalytic degradation process. Additionally, they have confirmed that with increasing ball-milling time and frequency, the photocatalytic role of nanocomposites becomes enhanced due to smaller particle size, greater surface area, and increased adsorption sites. Moreover, the best degradation temperature was 25 ˚C. Above this range, poor catalytic activity was owed to an unfeasible adsorption-desorption equilibrium between the $NiFe_2O_4$-rGO catalyst and MB dye molecules that led to larger desorption (Liang et al., 2018).

A charge transfer mechanism could account for the degradation of MB dye by using $NiFe_2O_4/Ag_3PO_4$ nanocomposites under visible light radiation provided by a 300 W Xe lamp. The photocatalytic capability was found to be greater for 5%-$NiFe_2O_4/Ag_3PO_4$ composites compared to all other wt.% of $NiFe_2O_4/Ag_3PO_4$ composites and bare Ag_3PO_4 (Fig. 7). At first, the production of holes and electrons took place in VB and CB by absorbing visible light. Afterwards, the electrons shifted from the CB of $NiFe_2O_4$ to Ag_3PO_4 because the CB potential of the former was more negative than that of the latter. Concurrently, holes migrated from the VB of Ag_3PO_4 to $NiFe_2O_4$, allowing the charge pair separation process to proceed. Consequently, the least chance of recombination of electrons and holes appeared, and thereby the holes in VB of $NiFe_2O_4$ took part in the oxidation of H_2O to form ȮH radicals. On the other hand, the involvement of electrons in the reduction process of O_2 to produce H_2O_2, which further generated ȮH radicals. Those active radical species made MB dye molecules decolorize and degrade to give degraded products (Zhao et al., 2016).

Coupling of nanorods $NiFe_2O_4$ with ZnO developed ZnO/$NiFe_2O_4$ nanocomposites and showed its photocatalytic ability towards MB dye degradation in presence of UV light as shown in Fig. 8. Experiments were conducted to degrade MB dye by performing various situations such as UV light alone in the absence of catalyst, 75 mg of ZnO/$NiFe_2O_4$ catalyst without UV radiation,75 mg of pure ZnO under UV illumination, and 75 mg of ZnO/$NiFe_2O_4$ catalyst under UV radiation. Among those conditions, the authors concluded that 75 mg of ZnO/$NiFe_2O_4$ nanocomposites as a catalyst under UV light accomplished better photocatalytic activity for the decolorization of 5×10^{-5} M concentration of MB dye. The mechanism behind that degradation process was adsorption of dye molecules to the catalytic surface, and charge transfer occurred between VB and CB of both $NiFe_2O$ and ZnO. In more detail, the transfer of photo-induced electrons happened from the CB of $NiFe_2O_4$ to ZnO through ZnO/$NiFe_2O_4$ interfaces. Simultaneously, the same number of holes shifted from the VB of ZnO to $NiFe_2O_4$ on behalf of $NiFe_2O_4$ nanorods placed with less positive CB potential and more negative VB potential compared to ZnO nanorods. The lifetime of those charge carriers increased as they reacted with O_2 and H_2O, producing active chemical ingredients such as $O_2^{\cdot-}$, ȮH radicals, and their anionic forms. All those chemical constituents helped to decolorize MB dye molecules into a non-dangerous product (Adeleke et al., 2018).

A ternary nanocomposite $TiO_2/NiFe_2O_4$/rGO was used for the decolorization of aqueous solutions containing MB dye molecules under UV and visible illumination. Adsorption of more MB dye molecules to the surface of nanocomposites took place on account of the higher GO amount (0.120 g) in nanocomposites favoured towards maximum removal efficiency. On the other hand, degradation under UV radiation performed well compared to visible illumination, as excitation of electrons progressed from VB to CB of TiO_2 in UV light. Another way to achieve maximum degradation has been achieved using H_2O_2 in order to produce ȮH radicals to be involved in the oxidation process. When radiation falls on $TiO_2/NiFe_2O_4$/rGO nanocomposites, light adsorption by TiO_2 produces holes in VB and electrons in CB of TiO_2. Those photo-induced charge carriers took part in the oxidation and reduction reactions and suppressed the recombination rate because of rGO, which performed a function as an electron acceptor. First of all, negative electrons in the CB of TiO_2 shifted to rGO, thereby reacting with O_2 to fabricate $O_2^{\cdot}$radicals. Secondly, the production of H_2O_2 happened by a reaction between the generated $O_2^{\cdot-}$ radicals and hydrogen ions. This in turn created ȮH radicals through the reduction process. Another way to assemble ȮH radicals was the reaction followed by positive holes and H_2O/OH. Thus, the mainly used active species were holes and ȮH radicals, which participated in the degradation of MB dye molecules into colourless, non-harmful products (Ziarati, Nadimi, and Ali, 2019).

An efficient catalyst, BiOBr/$NiFe_2O_4$ composites have been prepared by hydrothermal means for environmental remediation, mainly to chuck out MB dye from the water resources. The authors said that among the various weight percentages of $NiFe_2O_4$ coupled with BiOBr, BiOBr/$NiFe_2O_4$-20 % composites revealed the highest depletion of MB (90 % removal in 60 min). The production of electrons and holes was

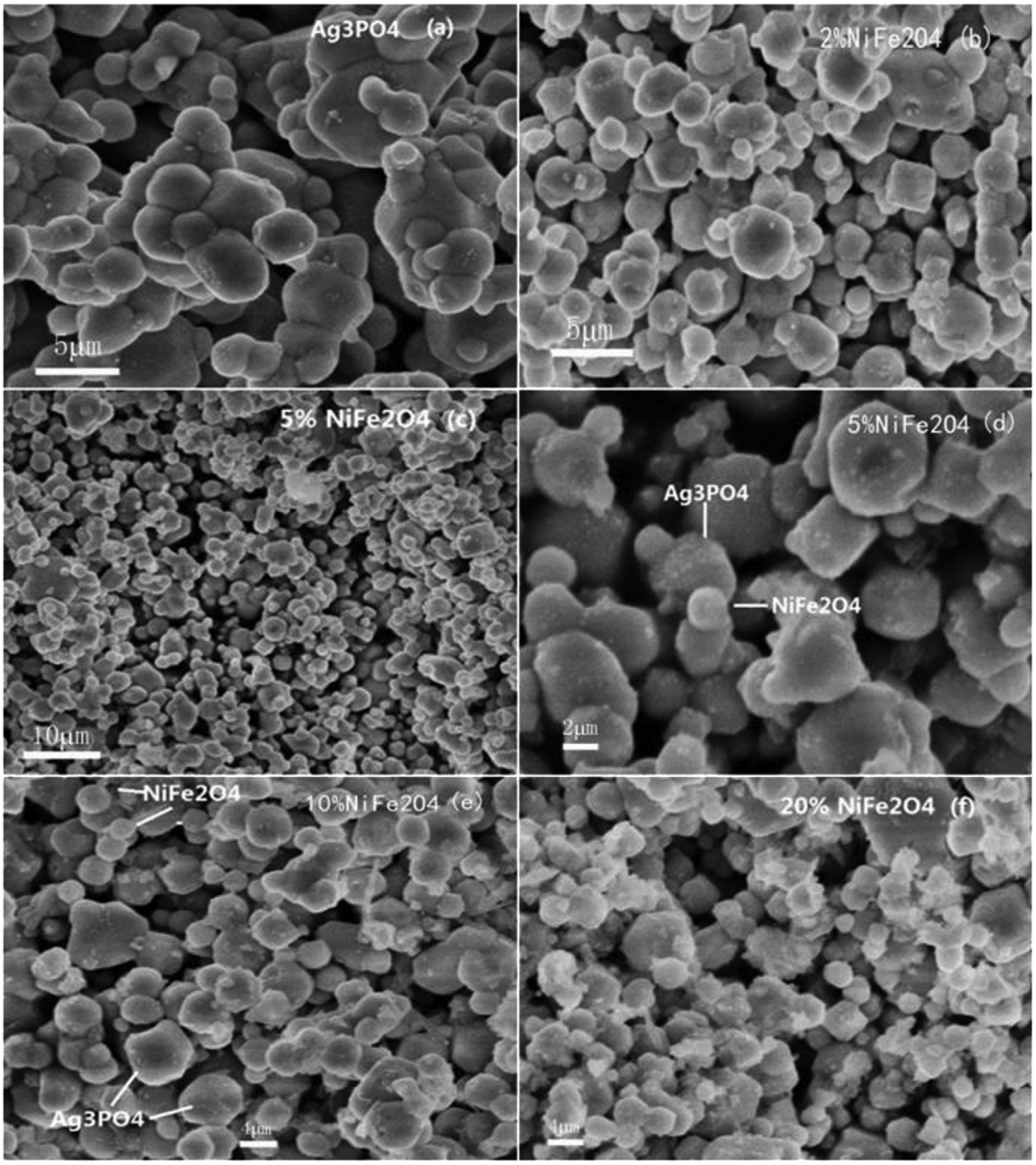

Fig. 7. SEM images of Ag_3PO_4 and $NiFe_2O_4/Ag_3PO_4$ composites with different contents: 2%, 5%, 10% and 20%. Reproduced with permission from ref (Zhao et al., 2016), copyright 2016, Elsevier.

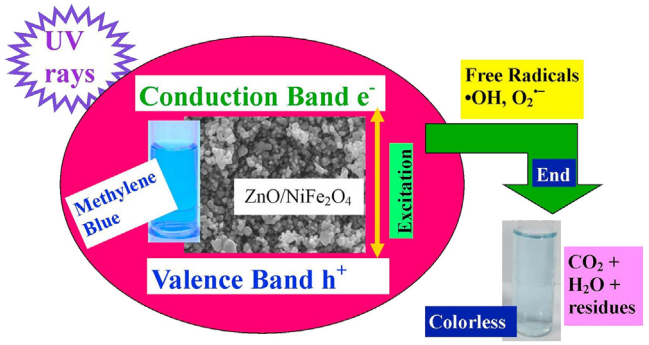

Fig. 8. Schematic diagram showing the photodegradation of MB using $ZnO/NiFe_2O_4$ as photocatalyst. Reproduced with permission from ref (Adeleke et al., 2018), copyright 2018, Elsevier.

achieved in the CB and VB of both BiOBr and $NiFe_2O_4$ due to the absorption of visible light by $BiOBr/NiFe_2O_4$. After that, the migration of electrons took place from more negative to less negative band edge potential in CB and, simultaneously, the holes shifted from more positive to less positive band edge potential in VB. Based on that, accumulation of a large number of negative electrons happened in CB of BiOBr and positive holes in VB of $NiFe_2O_4$, caused a greater charge separation and hence favoured the highest degradation of MB (Li et al., 2017).

4.2. Photocatalytic degradation of rhodamine B dye

Rhodamine B (RB), a water-soluble dye commonly used in the textile industry, is found to endanger the lives of aquatic organisms by creating a problem in their respiration. The breathing efficiency becomes sufficiently reduced and also causes a retardation in the photosynthetic capability, thereby creating an improper natural life for the living or-

ganisms in water bodies (Oyekanmi et al., 2019). Thus, the removal or degradation of RB from the water will provide the aquatic creatures with a safer and more peaceful life.

A different molar ratio of magnetic CdS-$NiFe_2O_4$ nanocomposites has been prepared and studied for its photocatalytic activity against RB dye under visible light conditions and showed an 85% removal efficiency in 120 min of contact time. The energy band gap value was around 2.18 eV for CdS-$NiFe_2O_4$ nanocomposites, less than that of pure CdS nanoparticles, which was around 2.33 eV, which inevitably promoted the highest degrading power of nanocomposites as a photocatalyst. The charge transfer mechanism played a significant role in the RB dye degradation process. Under the influence of visible light, the formation of holes and electrons occurred in the VB and CB of both CdS and $NiFe_2O_4$. After that, the immigration of photo electrons tended to flow from CdS CB to $NiFe_2O_4$ CB and, concurrently, photo-induced holes happened to move in the opposite direction, i.e., from $NiFe_2O_4$ VB to CdS VB. This movement was generated on account of more positive potential energy for CB and VB of $NiFe_2O_4$ compared to CB and VB of CdS. The lower the chance of recombination ability of charge carriers, the more enrichment for photocatalytic activity there is. Hence, those charge carriers participated in a reaction with atmospheric O_2 and H_2O to produce H_2O_2, and further reaction generated ȮH radicals led to the destruction of RB dye molecules into the safer products (Singh et al., 2017).

The silica coated $NiFe_2O_4$ nanocomposites that were synthesized through Stobber's method were used as photocatalysts towards RB dye removal and ensured that an increase in silica coating to $NiFe_2O_4$ retarded the photocatalytic activity. The diffusion of RB dye molecules to the catalytic surface of $NiFe_2O_4$ seemed difficult since silica acted as a barrier and caused the least production of ȮH radicals, thereby controlling the photocatalytic reaction (Singh et al., 2017). Different percentages of Ag_3PO_4/MIL-101/$NiFe_2O_4$ composites (10, 20 and 30 %) were used to degrade RB dye under visible radiation and it was found that maximum degradation (93 % removal in 30 min) was obtained for 20 % composition. In that, nanocomposite MIL-101, treated as MOF, acted as an electron carrier from Ag_3PO_4 to $NiFe_2O_4$. The lower band gap energy value (2.24 eV) and excess active sites of Ag_3PO_4/MIL-101/$NiFe_2O_4$ composites further enhanced the photo-degradation activity of RB dye in waste water. The addition of trapping agents during the course of the reaction created the lowest degradation rate, indeed mentioning that the role of $O_2^{\bullet-}$ radicals and positive holes encouraged the fastest degradation efficiency (Zhou et al., 2018).

To degrade 20 mL of 10 ppm of RB dye solution in the presence of solar light, 20 wt.% $NiFe_2O_4$@P-g-C_3N_4 nanocomposites showed superior photocatalytic activity compared to bare $NiFe_2O_4$, bare P-g-C_3N_4 and other wt.% compositions of the $NiFe_2O_4$@P-g-C_3N_4 catalyst. Nearly 98.8% colour degradation was achieved, and the kinetics were discovered to be first-order (Mishra et al., 2019). The enhanced photocatalytic properties of ternary $NiFe_2O_4$@TiO_2/rGO nanocomposites helped to degrade RB dye solution under UV radiation. During the photocatalytic process, rGO content in nanocomposites performed as an electron acceptor and the formation of π-conjugation occurred due to the presence of outermost electrons in carbon atoms. On absorption of UV light by nanocomposites, the involvement of photo-induced electrons of TiO_2 with H_2O and O_2 directed to the emergence of energetic active species, namely ȮH radicals, which attacked RB dye molecules. After the degradation process, the nanocomposites could be recovered using an external magnet and found to be stable for up to six cycles with a little loss in weight (Wang et al., 2018).

Degradation of RB dye molecules driven by visible light was studied using $NiFe_2O_4$ and $NiFe_2O_4$/rGO nanocomposites, and the results showed the degrading capacity was higher for $NiFe_2O_4$/rGO nanocomposites compared to bare $NiFe_2O_4$. GO content of 40 mg in $NiFe_2O_4$/rGO nanocomposites played a superior role in the degradation process, and further increase in rGO content revealed the lowest degradation performance. This had happened owing to the shielding/screening effect of graphene, which in turn caused difficulty in light penetration towards the catalytic surface and thus proved that the rGO amount in $NiFe_2O_4$/rGO nanocomposites played a vital role in determining the photocatalytic proficiency. As shown in Fig. 9, the addition of Pd to $NiFe_2O_4$/rGO to prepare ternary Pd-$NiFe_2O_4$/rGO nanocomposites revealed that 70 mg GO content in Pd-$NiFe_2O_4$/rGO exhibited the highest degradation rate in a shorter time compared to 40 mg rGO in $NiFe_2O_4$/rGO and in those ternary nanocomposites, the part of Pd was only a co-catalyst. Because of the versatility of Pd-$NiFe_2O_4$/rGO nanocomposites, authors investigated not only the degradation of RB dye solution, but also how to degrade MO and MB dyes in the presence of visible light for water purification (Li et al., 2016).

When compared to pure $NiFe_2O_4$, g-CN, binary nanocomposites $NiFe_2O_4$/5 g-CN, and all other wt.% of CD, ternary nanocomposites $NiFe_2O_4$/5 g-CN/7.5 CD demonstrated superior photocatalytic performance to degrade RB dye solution under conditions such as LED illumination, in the presence of H_2O_2, and at pH 6.3. Those were accredited to the formation of synergistic effects between $NiFe_2O_4$ nanoparticles and g-CN, and, moreover, the addition of CD created a rise in the production of photo-induced charge carriers. Consequently, this led to a decrease in recombination rate, thereby favouring the highest removal efficiency. The authors proposed that during the degradation process of RB dye molecules, the mechanism followed by type-II heterojunction into Z-scheme conversion. Elemental trapping experiments were conducted using scavengers like benzoquinone, isopropyl alcohol, and ethylene diamine tetraacetic acid to clarify the involvement of active radical species, namely $O_2^{\bullet-}$ and ȮH radical. Further, the supporting evidence for the formation of energetic species were obtained by undertaking nitroblue tetrazolium and terephthalic acid tests on photocatalytic nanocomposites (Palanivel and Mani, 2020).

Under the influence of visible light illumination, a heterojunction photocatalyst BiOBr/$NiFe_2O_4$ was synthesized and followed the charge transfer process to decompose the modern pollutant RB. In order to enclose the active species involved in the degradation mechanism of RB dye, trapping experiments were conducted using various scavengers, which gave the justification that positive holes and $O_2^{\bullet-}$ radicals were the main species taking part in that process. Moreover, BiOBr/$NiFe_2O_4$ nanocomposites revealed the maximum current density that led to the extreme separation of charge carriers and, in that way, caused a delay in the recombination process. Additionally, the size of $NiFe_2O_4$ nanoparticles was found to be smaller and the mode of contact of $NiFe_2O_4$ with BiOBr nanosheets was "point-plane". Thus, all of the aforementioned factors contribute to the enhanced removal of modern dye from contaminated water resources via photocatalytic processes (Li et al., 2018). 100% RB degradation was achieved using a semiconductor-based ternary photocatalyst PANI/Ag_3PO_4/$NiFe_2O_4$ upon visible light treatment by following a double Z-scheme charge transfer mechanism. Absorption of visible light by PANI/Ag_3PO_4/$NiFe_2O_4$ nanocomposites tended to fabricate electrons in CB and holes in VB of all the three individuals of nanocomposites. After that, those electrons in CB of Ag_3PO_4 shifted towards VB of $NiFe_2O_4$ through PANI and HUMO of PANI via metallic Ag, which then remerged with the holes. Furthermore, the formation of $O_2^{\bullet-}$ species from O_2 happened by reacting with electrons that had stronger reduction potential and got accumulated on the LUMO of PANI and the CB of $NiFe_2O_4$. Furthermore, because the Ag_3PO_4 CB potential was more negative than E^0 (O_2/H_2O_2), H_2O_2 was produced as a result of O_2 interaction with Ag_3PO_4 CB electrons, as shown in Fig. 10. As a result, the H_2O_2 reacts with the positive holes accumulated in the VB of Ag_3PO_4, causing the dye compound to degrade. The photocorrosion of Ag_3PO_4 became highly reduced owing to the immigration of electrons from its surface and was favoured for the improved photocatalytic activity of nanocomposites (Chen et al., 2019).

Under the influence of visible light radiation, it has been found that the complete degradation of RB (10 mg/L, pH 7) was attained after 60 min of contact time of dye molecules with Ag/AgBr/$NiFe_2O_4$ composites as a photocatalyst. Moreover, Ag/AgBr/$NiFe_2O_4$ showed better photocatalytic activity compared to pure $NiFe_2O_4$ and Ag/AgBr and also in-

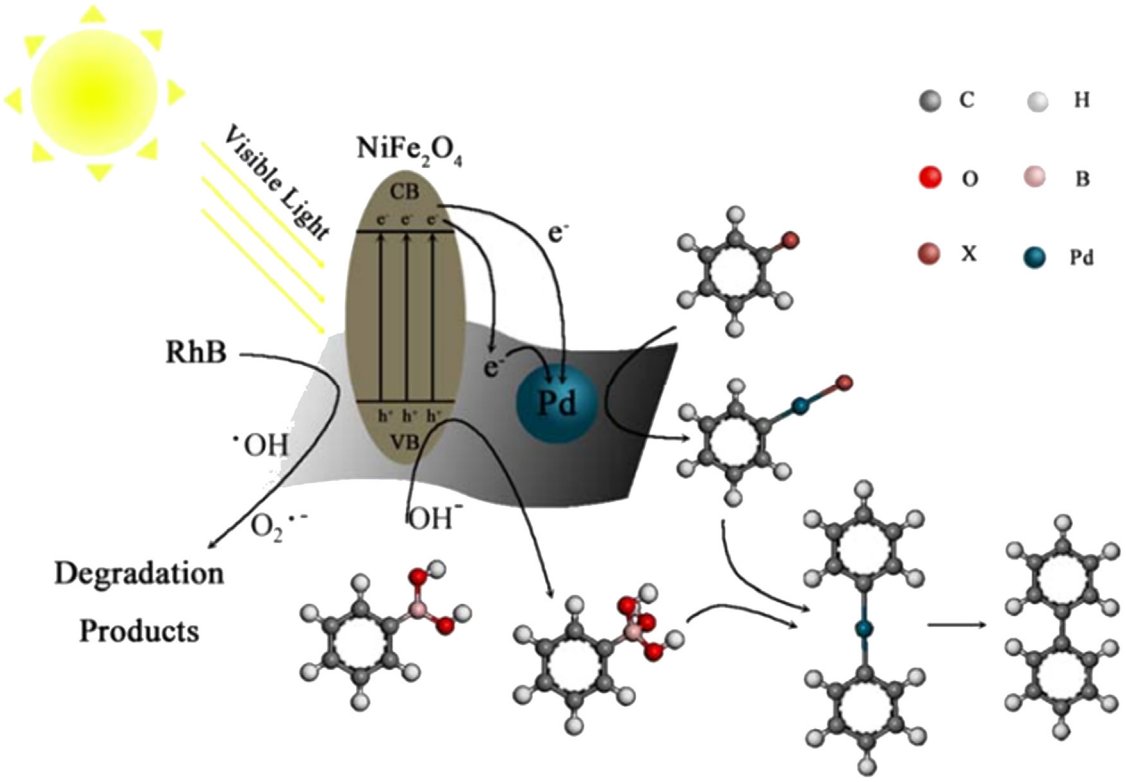

Fig. 9. The schematic diagram of the possible photocatalytic mechanism over the Pd-$NiFe_2O_4$/rGO nanocomposite photocatalyst. Reproduced with permission from ref (Li et al., 2016), copyright 2016, Elsevier.

creased the degradation efficiency. The major active species involved in the photocatalytic process were O_2^- which have been confirmed by using ascorbic acid as a radical scavenger via radical trapping experiments. The creation of charge carriers upon the absorption of light and the movement process took place based on energy difference. This in turn produced the migration of electrons from CB of $NiFe_2O_4$ to CB of AgBr and, likewise, the holes shifted to VB of $NiFe_2O_4$ from VB of AgBr. Additionally, the flow of electrons from surface plasmon resonance (SPR) of Ag nanoparticles to CB of AgBr has been generated because of the superior work function of AgBr (5.3 eV) compared with Ag (4.25 eV) as shown in Fig. 11. Therefore, those assembled electrons reacted with O_2 to create O_2^- radicals, which were involved in the decomposition of RB dye molecules into a non-toxic chemical product (Ge et al., 2017).

The N-doped TiO_2/$NiFe_2O_4$/diatomite (NND), a ternary hybrid composite, functioned as a photocatalyst to eradicate RB dye solution from the contaminated water. During the composite preparation, particularly in which N doped TiO_2 synthesis, the nitrogen (N) source came from urea (2.8 g) denoted as 2-NND, revealed better photocatalytic performance compared to 1-NND (1.4 g), 3-NND (4.2 g), 4-NND (5.6 g), TiO2/$NiFe_2O_4$/diatomite, N doped TiO_2/diatomite, N doped TiO_2 and $NiFe_2O_4$/diatomite. The enhanced photocatalytic efficiency of 2-NND was attributed to the effect of synergy formation between diatomite and N-doped TiO_2, which led to further adsorption and degradation processes. Moreover, PL analysis verified the synergistic actions developed between $NiFe_2O_4$ and N-doped TiO_2. The above two factors created a delay in the recombination rate of charge carriers, thereby favouring an improvement in the overall photocatalytic process and carried out the radical trapping experiments, which showed the major active chemical species to be O_2^- (Chen and Liu, 2017).

$NiFe_2O_4$ nanoplates formed a collaboration with SQD to create $NiFe_2O_4$/SQD (NFS) nanocomposites to be involved in the elimination process of RB dye molecules from contaminated water resources for better water treatment. The authors discovered that NFS-10 (10 mg SQD) nanocomposites showed 98% degradation of RB after visible-light radiation for 105 min due to p-n heterojunction formation between $NiFe_2O_4$ and SQD. That formation could cause a delay in the recombination process of charge carriers, thereby creating an enhancement in the photocatalytic activity of nanocomposites. The proposed mechanism for the decomposition of RB dye molecules in the presence of visible light was illustrated in the following reactions.

$$NiFe_2O_4/SQD + * \left(visible - light\ \ radiation\right) \rightarrow NiFe_2O_4\left(e_{CB}^- + h_{VB}^+\right)/SQD$$

$$NiFe_2O_4\left(e_{CB}^- + h_{VB}^+\right)/SQD \rightarrow NiFe_2O_4\left(h_{VB}^+\right)/SQD\left(e_{CB}^-\right)$$

$$SQD\left(e_{CB}^-\right) + O_2 \rightarrow O_2^{\cdot -}$$

$$2SQD\left(e_{CB}^-\right) + O_2 + 2H^+ \rightarrow H_2O_2$$

$$H_2O_2 + O_2^{\cdot -} \rightarrow OH^{\cdot} + OH^- + O_2$$

$$OH^{\cdot} + RB \rightarrow major\ \ degradation\ \ products$$

$$O_2^{\cdot -} + RB \rightarrow minor\ \ degradation\ \ products$$

$NiFe_2O_4(h^+{}_{VB})$ + RB → major degradation products (Babu et al., 2020).

AgBr/$NiFe_2O_4$ composites proved to be an efficient photocatalyst to degrade Rh B dye molecules with the influence of visible light (10 W LED lamp – source of visible light) to safeguard our water resources. The decomposition of RB after 60 min irradiation with the light source was found to increase in the following order $NiFe_2O_4$ < AgBr < AgBr/$NiFe_2O_4$. The least performance of $NiFe_2O_4$ as a photocatalyst was ascertained due to the difficulty in the movement of charge carriers in $NiFe_2O_4$. Therefore, an enhancement in the photocatalytic activity of

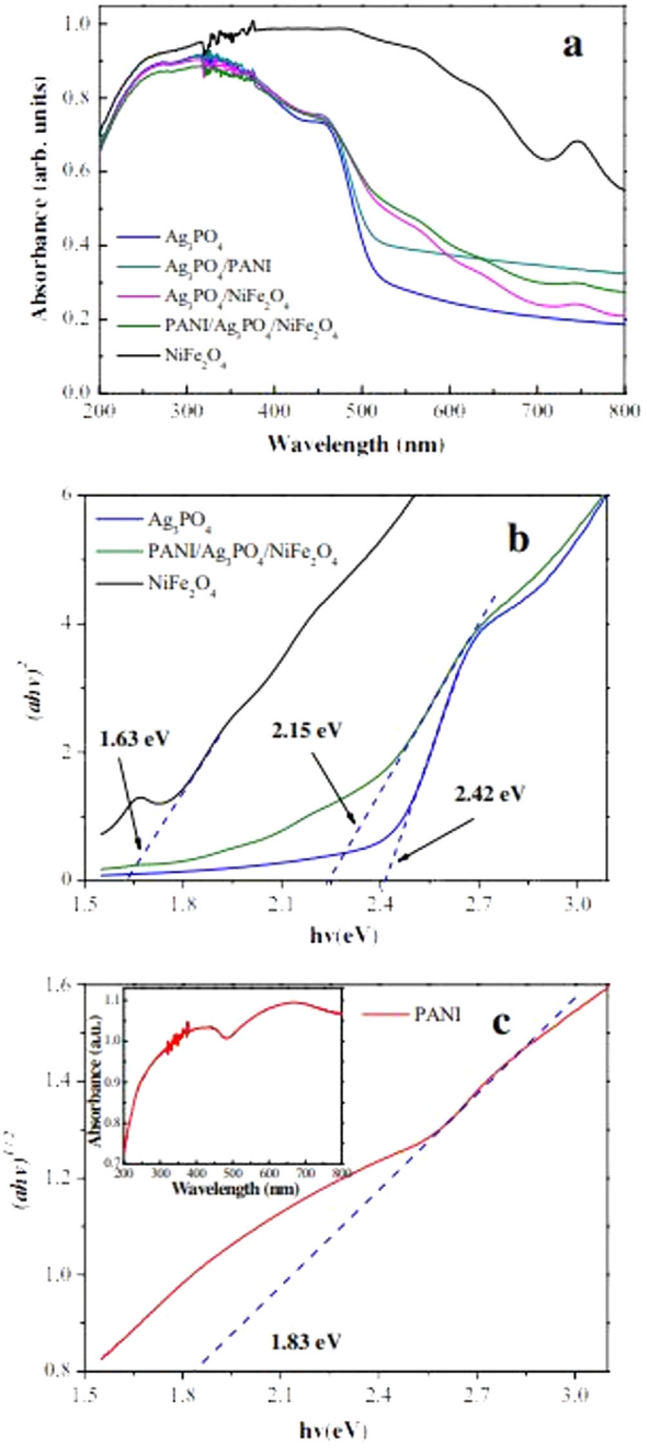

Fig. 10. UV-vis DRS spectra of $NiFe_2O_4$, Ag_3PO_4, $Ag_3PO_4/NiFe_2O_4$, Ag_3PO_4/PANI and PANI/$Ag_3PO_4/NiFe_2O_4$ composites (a); and the plots of $(\alpha h\nu)^2$ vs. hν for $NiFe_2O_4$, Ag_3PO_4 and PANI/$Ag_3PO_4/NiFe_2O_4$ composites (b); and the plots of $(\alpha h\nu)^{1/2}$ vs. hν PANI (c). Reproduced with permission from ref (Chen et al., 2019), copyright 2019, Elsevier.

$NiFe_2O_4$ was achieved by blending with AgBr to generate AgBr/$NiFe_2O_4$ composites whose surface area were higher than those that had been confirmed by conducting BET analysis. Using benzoquinone as a radical trapping agent, it was confirmed that $O_2^{\cdot-}$ radicals played a major role in eliminating the pollutant RB from the contaminated water (Ge and Hu, 2016).

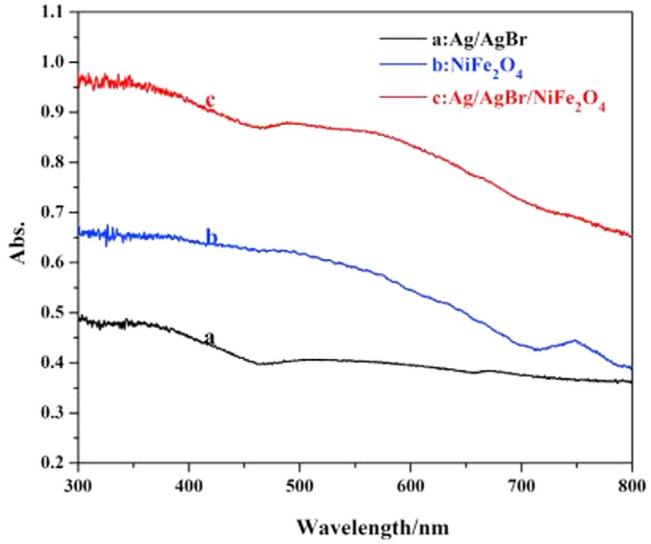

Fig. 11. The UV-vis diffuse reflectance spectra of the as-synthesized samples. Reproduced with permission from ref (Ge et al., 2017), copyright 2017, Elsevier.

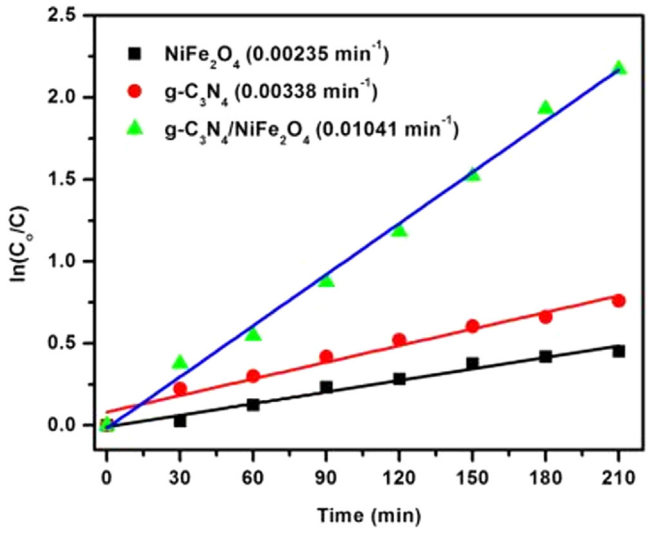

Fig. 12. The degradation rate constant (k_{ap}) of MO over the pure $NiFe_2O_4$, pure g-C_3N_4 and g-$C_3N_4/NiFe_2O_4$ nanocomposites. Reproduced with permission from ref (Gebreslassie et al., 2019), copyright 2019, John Wiley and Sons.

4.3. Photocatalytic degradation of methyl orange dye

An anionic dye, MO, comes under the azo dye group category. The presence of MO in water creates a huge risk for humans, such as chronic health issues, tissue necrosis, cyanosis, vomiting and jaundice, and at the same time endangers the lives of aquatic species (Zhai et al., 2018, Darwish, Rashad, and AL-Aoh, 2019, Uddin and Baig, 2019). Hence, for the betterment of life and protection, the removal of MO dye from the contaminated water has to be carried out.

Photocatalytic removal of MO dye from an aqueous solution was studied using g-$C_3N_4/NiFe_2O_4$ nanocomposites under visible light radiation. Fig. 12 shows that when compared to pure $NiFe_2O_4$ and g-C_3N_4, 100 % removal of MO dye was achieved using g-$C_3N_4/NiFe_2O_4$ after 210 min, and the kinetics followed to be pseudo first-order. The photocatalyst's stability was maintained at good for three consecutive cycles, and this was confirmed by taking SEM images of nanocomposites before and after the degradation process, which revealed no change in morphology (Gebreslassie et al., 2019). TiO_2, metallic Ag, and

$NiFe_2O_4$ nanoparticles were used to create two- and three-component heterostructures. The prepared samples include $TiO_2/NiFe_2O_4$, TiO_2-Ag, $TiO_2/NiFe_2O_4$/Ag, and TiO_2-Ag/$NiFe_2O_4$. Among these four samples, the TiO_2-Ag/$NiFe_2O_4$ heterostructure as a photocatalyst showed greater efficiency of MO dye removal under visible irradiation using an LED light source for two hours. In that heterostructure, Ag content was very negligible and acted as a sensitizer and also as an electron scavenger. Migration as well as charge separation took place to a greater extent across the interfaces, prompting a vectorial pathway of electrons from $NiFe_2O_4$ to TiO_2 and then to Ag. Additionally, the development of internal electric fields favoured the separation of charges, and that in turn enhanced the photo-decomposition of MO for water remediation (Online et al., 2016).

The greener way of synthesizing nanocomposites is an environmentally friendly process and a most welcome field to degrade organic pollutants from wastewater. Herein, an attempt has been made to synthesize $NiTiO_3/NiFe_2O_4$ nanocomposites using onion extract as a reducing and capping agent by following the sol-gel auto-combustion method. MO dye was treated as a photocatalyst to degrade in the presence of a mercury lamp as a light source to provide UV radiation. Various molar ratios of Ti/Ni comprising 1:1, 1:2, and 2:1 of composites have been prepared and the optimum condition ratio was 1:1, which showed an 88 % degradation efficiency of MO dye after one-hour exposure of the dye solution under UV light (Ansari, Bazarganipour, and Salavati-niasari, 2016). Removal of MO dye from water under visible light has been achieved by using γ-Fe_2O_3@$NiFe_2O_4$ composites which followed an adsorption-cum photodegradation process. Almost 98.2 % of MO dye molecules were eliminated owing to the adsorption of dye molecules to the surface of composites in dark conditions for 30 min, because of the vast surface area of γ-Fe_2O_3@$NiFe_2O_4$ that had been confirmed by the BET analysis study. After that, complete degradation was attained within 60 min of contact time under visible light illumination established by the vanishing of three absorption peaks of MO. Enrichment in that process was accredited to the long lifetime of electron-hole pairs and the delay in recombination rate. Further evidence for the photocatalytic degradation process came from the performance of active species, which made MO dye molecules break down into carboxylic acids. As a result, γ-Fe_2O_3@$NiFe_2O_4$ composites could be used as an efficient photocatalyst for the degradation of organic pollutants in wastewater (Borhan, Gherca, and Iordan, 2019).

G. Gebreslassie et al., prepared a ternary nanocomposites g-C_3N_4/graphene/$NiFe_2O_4$ to eradicate MO dye under the influence of visible light by following the photocatalytic process. Results showed that 100 % removal of MO was achieved using g-C_3N_4/graphene/$NiFe_2O_4$-25 % (CGN-25 %) photocatalyst in 120 min. However, the performance of pure $NiFe_2O_4$, pristine g-C_3N_4 and g-C_3N_4/$NiFe_2O_4$-25 % (CN-25 %) as a photocatalyst towards dye degradation was found to be low. The proposed mechanism for this photocatalytic process was z-scheme charge transfer and separation of photo-induced charge carriers accomplished using visible light radiation. With the help of graphene as an electron mediator, the shifting of electrons from CB of $NiFe_2O_4$ to VB of g-C_3N_4 had been taken place, which then caused the separation of electrons and holes in CB of g-C_3N_4 and VB of $NiFe_2O_4$ respectively. Due to that, the highest reduction power of electrons and the highest oxidation power of holes became grouped at CB of g-C_3N_4 and VB of $NiFe_2O_4$ respectively. After that, the holes involve in a reaction with H_2O molecules to produce ȮH radicals and simultaneously, electrons reacted with O_2 to form $O_2^{\bullet-}$. Thus, the two main reactive radicals involved in MO dye degradation were OH˙ and $O_2^{\bullet-}$ (Gebreslassie et al., 2019).

4.4. Photocatalytic degradation of congo red dye

An anionic diazo dye, CR, creates severe health problems for the living creatures when it gets blown into the bodies of water from the dye-based industries. The CR dye has the ability to cause carcinogenic diseases, vomiting, nausea, and diarrhoea (Liu et al., 2019, Jabar et al., 2020). Moreover, the presence of a very low concentration of CR dye puts the life of aquatic individuals in critical condition (Mondal and Kar, 2018). Thus, a major cure has to be considered for the destruction of CR dye from the polluted water environment.

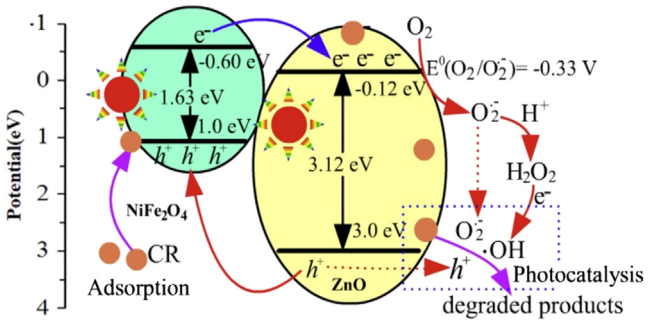

Fig. 13. Photocatalytic mechanism of CR dye eradication using $NiFe_2O_4$/ZnO. Reproduced with permission from ref (Zhu et al., 2016), copyright 2016, Elsevier.

Degradation of CR dye under sunlight has been achieved by using $NiFe_2O_4$/ZnO hybrids, which was shown in Fig. 13. The photocatalyst absorbed sunlight, creating positive holes in VB and electrons in CB of both $NiFe_2O_4$ and ZnO. After that, those holes were transferred from the VB of ZnO to $NiFe_2O_4$, since the VB potential of $NiFe_2O_4$ was less positive than that of ZnO. Simultaneously, electrons moved from the CB of $NiFe_2O_4$ to ZnO since the CB potential of ZnO was less negative than that of $NiFe_2O_4$. These charge carriers reacted with O_2 and H_2O in aqueous solution to form reactive species, specifically $O_2^{\bullet-}$, ȮH, and OH which inevitably aided the photocatalytic degradation process (Zhu et al., 2016).

Microwave treatment was applied to prepare $NiFe_2O_4$-NiO nanocomposites from their corresponding metal chlorides and nitrates in basic pH conditions and aimed to degrade CR dye through photocatalytic activity under UV radiation. CR dye solution was prepared at pH 3 and 5, and found that the contact of CR dye solution with $NiFe_2O_4$-NiO nanocomposites for one hour created decolorization of 100 % for pH 5 and 66.5 % for pH 3, respectively. The superior performance of $NiFe_2O_4$-NiO nanocomposites compared to NiO was attributed to the slow recombination rate of negative electron and positive hole pairs (Saffarzadeh, Nabiyouni, and Heidary, 2019).

4.5. Photodegradation of phenol

Phenol, the major organic and toxic pollutant, has an adverse effect on humans (Singh et al., 2019, Tian et al., 2018). In particular, when it comes in contact with the skin, it can be readily absorbed, leading to irritation. On the other hand, it may cause changes in endocrine systems. Additionally, the discharge of phenol into the chlorinated water reacts to form various chlorinated phenolic compounds, which are still harmful (Scott et al., 2019). Thus, the step towards the degradation of phenol from the polluted surroundings has to be directed towards the environment's concern.

Degradation of phenol under solar light was achieved using $NiFe_2O_4$@P-g-C_3N_4 nanocomposites and it was found that an increase in $NiFe_2O_4$ by 20 wt.% in nanocomposites, i.e., 20 wt.% $NiFe_2O_4$@P-g-C_3N_4 displayed better photocatalytic performance under ambient reaction conditions. Further increase in $NiFe_2O_4$ content exhibited the lowest photocatalytic performance, which was assigned to more occupation of $NiFe_2O_4$ on the surface of the photocatalyst, thereby increasing the difficulty of solar light penetration into the catalyst surface. The proposed mechanism for phenol degradation was the Z-scheme charge transfer mechanism, in which there was the creation of photoexcited electrons and holes in the presence of solar light. Since the positive po-

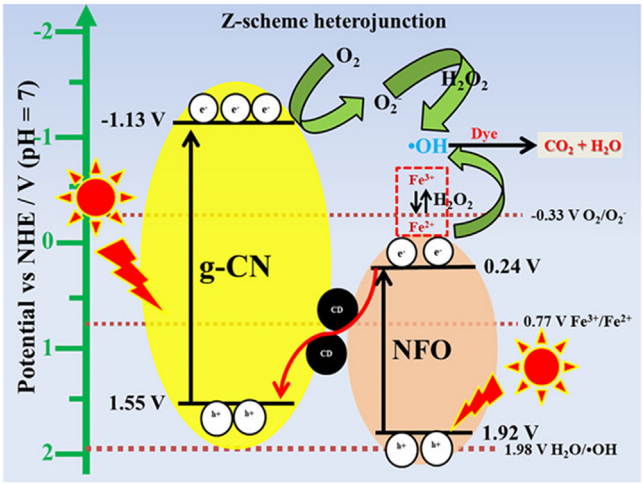

Fig. 14. Schematic presentation of the Photo-Fenton degradation of organic dyes. Adapted from ref (Palanivel and Mani, 2020), Copyright 2020, American Chemical Society.

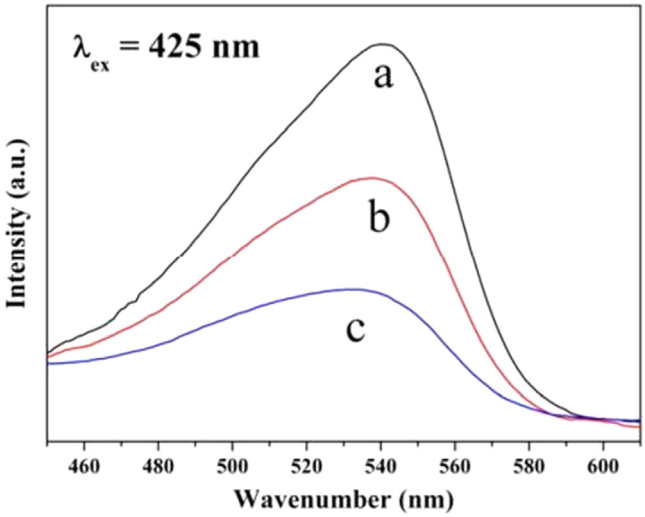

Fig. 15. PL spectra of (a) pure $NiFe_2O_4$, (b) $NiFe_2O_4$/rGO-4, (c) Pd-$NiFe_2O_4$/rGO-4 upon 425 nm excitation. Reproduced with permission from ref (Li et al., 2016), copyright 2016, Elsevier.

tential was less for $NiFe_2O_4$ compared to P-g-C_3N_4, the flow of photoexcited electrons took place from CB of $NiFe_2O_4$ to VB of P-g-C_3N_4. Subsequently, those electrons in VB of P-g-C_3N_4 got shifted to CB of P-g-C_3N_4, where they captured O_2 to produce $O_2^{\cdot-}$ anion. The positive holes that were left in the VB of $NiFe_2O_4$ reacted with H_2O to form H^+ and ȮH radical. The formation of those active species like $O_2^{\cdot-}$ and ȮH reacted with phenol to form degraded products which were not detrimental. The chief active species involved in the above mechanism was ȮH which had been confirmed by doing trapping experiments. Finally, the authors concluded that the harmful organic pollutant phenol was converted into non-harmful products using $NiFe_2O_4$@P-g-C_3N_4 nanocomposites (Mishra et al., 2019). Similarly, the photo-degradation of organic dyes were also studied by using $NiFe_2O_4$ (NFO)/graphitic carbon nitride (g-C_3N_4, g-CN) catalyst and the proposed reaction mechanism was shown in Fig .14 (Palanivel and Mani, 2020).

The performance of photocatalysts, namely $NiFe_2O_4$, $NiFe_2O_4$/rGO (40 mg of GO) and Pd-$NiFe_2O_4$/rGO (70 mg of GO) were studied towards the degradation of phenol in the presence of visible light irradiation for one hour. Among those aforesaid materials, the highest degradation rate of phenol was achieved using Pd-$NiFe_2O_4$/rGO nanocomposites, and the aspects supported to enhance the photocatalytic action were accomplished because of the larger surface area and pore volumes of nanocomposites, and also by using powerful visible light illumination. Another supported evidence for the higher photocatalytic performance attained from PL spectra which showed a reduction in PL signal as shown in Fig. 15. That was attributed to the trapping of photo-induced electrons by rGO and Pd, and thus restricted the recombination of charge carriers. Further, the trapping experiments were performed to indicate the presence of active species (Li et al., 2016).

4.6. Photodegradation of antibiotics

Due to the growth of pharmacy-based industries for the welfare of humans and farm animals, the usage of antibiotics has been greatly increased (Zhang et al., 2020). At the same time, poor metabolism has been encountered in antibiotics (especially like tetracycline), and so their presence in this biodiversity facilitates the production of serious chronic and health hazards (Wang et al., 2020, Cao et al., 2019). Therefore, an effort has been made by the researchers to violate antibiotics to a greater level.

Tetracycline (TC), an antibiotic considered to be an organic pollutant, was degraded by using binary $NiFe_2O_4$/5 g-CN and ternary $NiFe_2O_4$/5 g-CN/7.5 CD nanocomposites (Fig. 16). Under the influ-

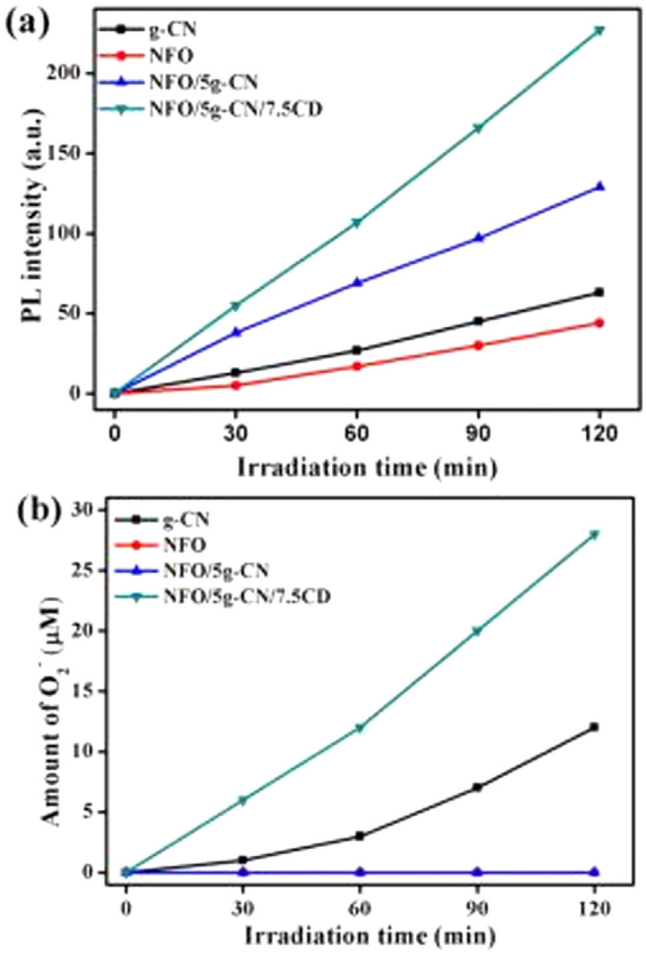

Fig. 16. (a) Terephthalic acid (TA) test and (b) nitroblue tetrazolium (NBT) test. Adopted from ref (Palanivel and Mani, 2020), Copyright 2020, American Chemical Society.

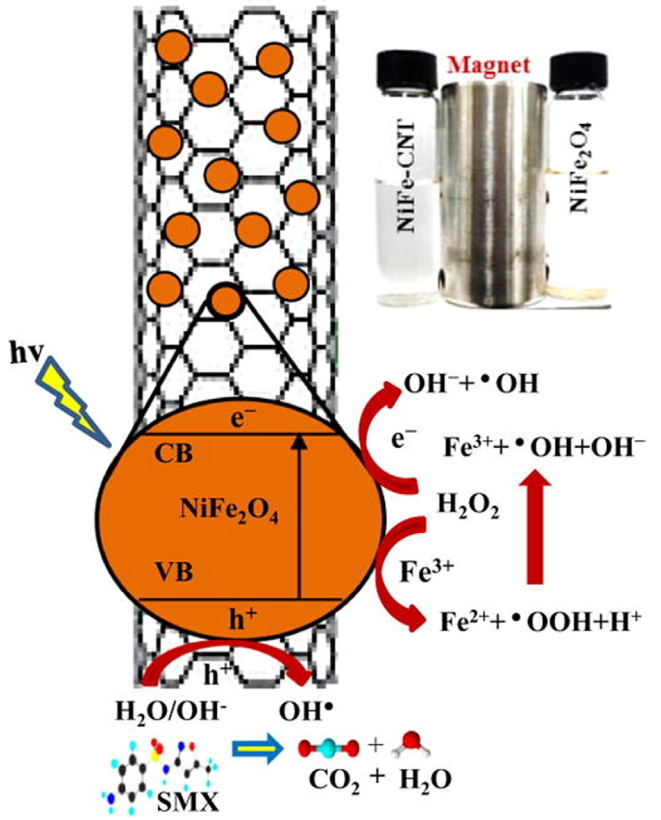

Fig. 17. Schematic diagram of SMX degradation using $NiFe_2O_4$-CNT. Reproduced with permission from ref (Nawaz et al., 2020), copyright 2020, Elsevier.

ence of LED radiation, binary composites showed a type-II heterojunction mechanism and ternary composites displayed a Z-scheme pathway. When light rays struck the surface of $NiFe_2O_4$/5 g-CN/7.5 CD photocatalyst nanocomposites, electrons moved from the CB of $NiFe_2O_4$ to the VB of g-CN via the surface of CD. After that, those electrons got excited to the CB of g-CN by absorbing light and reacted with O_2 to produce $O_2^{\cdot -}$ radicals. This in turn reacted with H_2O_2 to create ȮH radicals through a process called the Haber-Weiss reaction. Eventually, on account of the more negative potential energy of $NiFe_2O_4$ in CB, by a photo-reduction process, Fe^{3+} ions were reduced into Fe^{2+} ions. Accordingly, the creation of ȮH radical species occurred through the involvement of Fe^{2+} ions with H_2O_2 and, simultaneously, Fe^{2+} ions oxidized into Fe^{3+} by reacting with H_2O_2. Because of the large amount of active ȮH radicals produced, the TC pollutant degraded into harmless products (Palanivel and Mani, 2020).

$NiFe_2O_4$-CNT composite, an excellent choice of photocatalyst was used to degrade an organic pollutant, sulfamethoxazole (SMX) in the presence of ultraviolet-A (UV-A) and visible radiation as illustrated in Fig. 17. The proposed mechanism for the degradation of SMX from waste water was the photo-Fenton process. The incorporation of 25 % wt.% of CNTs into $NiFe_2O_4$, two hours of composite contact time with SMX, the presence of 1 µL/mL of H_2O_2, a 0.025 g/L amount of $NiFe_2O_4$-CNT and an acidic pH, all favoured the higher photocatalytic degradation of 5 mg/L of SMX. The involvement of ȮH radicals played a major role in the degradation process which had been produced in two ways. First of all, the light rays fell on the photocatalytic surface and created photo-generated holes and electrons. After that, those electrons in CB reacted with H_2O_2 to form ȮH radicals. Concurrently, holes in VB mingled with H_2O and OH⁻ to produce ȮH radicals. On the other hand, $O_2^{\cdot -}$ radicals were also formed during this process, but their contribution was low compared to ȮH radicals. Further confirmation of the involvement of those active chemical species has been obtained by performing trapping experiments using scavengers. In that process, conversion of SMX into CO_2, H_2O, sulphate ions, ammonium ions, nitrate ions, and mineral acids was achieved through seven intermediates and found to be less toxic, which had been confirmed by toxicity analysis (Nawaz et al., 2020).

The complete degradation of a powerful antibiotic named oxytetracycline (OTC) was achieved using graphitic carbon nitride/$NiFe_2O_4$ (GCN/$NiFe_2O_4$) composites under solar radiation. Higher removal of OTC was achieved in the presence of visible light and adsorption via photocatalysis (A+P) process than in the absence of light (DA) and adsorption followed by photodegradation (A-P) processes. When the photocatalytic composites GCN/$NiFe_2O_4$ were irradiated with solar light, there would be the construction of holes and electrons in VB and CB of both GCN and $NiFe_2O_4$. Thereupon, the migration of holes happened from VB of GCN to VB of $NiFe_2O_4$, since the former had a larger positive potential energy in VB. Conversely, the movement of electrons from CB of $NiFe_2O_4$ to CB of GCN takes place due to the lower negative potential energy in CB of GCN. The shifting of charge carriers created a greater separation of charges and a delayed rate of recombination, thereby making ȮH radicals production lead to complete mineralization of OTC into non-harmful products. The photocatalyst could be easily recovered by means of a magnet and able to prove its stability even up to 10 cycles, thus being verified as an efficient composite to degrade OTC antibiotics from waste water (Sudhaik et al., 2018).

The powerful antibiotics ampicillin and OTC were entirely mineralized in the presence of two photocatalysts, namely $NiFe_2O_4$/graphene sand composite ($NiFe_2O_4$/GSC) and $NiFe_2O_4$/bentonite ($NiFe_2O_4$/BT) under solar illumination. The enhanced removal of AMP and OTC was achieved by the adsorption of antibiotics onto the photocatalytic surfaces ($NiFe_2O_4$/GSC and $NiFe_2O_4$/BT) and simultaneously undertook a photodegradation process which could be mentioned as the A+P process (Gautam et al., 2016). Eradication of an antibiotic OTC was executed using Ce-doped TiO_2/$NiFe_2O_4$/diatomite (CTND), a ternary composite which acted as a photocatalyst along with the support of visible light radiation. CTND-2 (0.05 g of $Ce(NO_3)_3$ had been used during synthesis) revealed better photocatalytic activity towards OTC degradation, on account of considerable surface area compared to other photocatalysts such as CTND-1 (0.02 g), CTND-3 (0.1 g), CTND-4 (0.2 g), Ce-TiO_2/diatomite, Ce-TiO_2, TiO_2/$NiFe_2O_4$/diatomite and $NiFe_2O_4$/diatomite. The introduction of Ce and diatomite in CTND composites provided a decrease in TiO_2 energy band gap by means of the development of an intra-band structure and acted as supporters, respectively. The degradation mechanism of OTC could be described step by step. First of all, OTC got adsorbed to the catalytic surface CTND and then, by absorbing visible light, the formation of holes and electrons tended to happen in Ce-TiO_2 VB and CB, respectively. After that, the immigration of electrons from CB of Ce-TiO_2 to CB of $NiFe_2O_4$ took place since the latter CB material had less energy compared to the former. Those electrons then fell down to the VB of $NiFe_2O_4$ and passed into the VB of Ce-TiO_2. This complete cyclic process created a delay in recombination of charge carriers and thereby increased the photocatalytic efficiency of composite CTND (Chen and Liu, 2017).

An organic pollutant TC has been expelled from the waste water with the aid of a ternary hybrid composite named Ce/N co-doped TiO_2/$NiFe_2O_4$/diatomite (CN-TND) prepared through the sol-gel method. It has been found that using CN-TND-2 (0.05 g of Ce $(NO_3)_3.6H_2O$) as a catalyst, the degrading proportion of TC became 24.2 % under dark conditions and 83.6 % under visible light radiation conditions during 90 min of contact time of the catalyst with the TC. The advantage of the Ce and N doped hybrid composite was to provide a lower band gap energy value of TiO_2 to form an intra-band structure, which in turn facilitated the generation of photo-induced charge carriers. After that, a cyclic charge transfer process takes place to produce a delay in recombination rate favoured towards photo-degradation of TC. Finally, the formation of active species occurred through the interaction of holes and electrons with O_2 and H_2O. Those TC molecules

Table 2
Types of $NiFe_2O_4$-based nanocomposites used to degrade the organic pollutant from the polluted water

Organic pollutant	$NiFe_2O_4$-based nanocomposites	Light source	Initial concentration of pollutant	Catalyst dosage	Degradation efficiency in %	Time taken for degradation in min	Main active species	References
TC	$NiFe_2O_4/ZnWO_4$	Solar light	-	-	98	105	O_2^-, ȮH	Reddy et al., 2020
RB	$NiFe_2O_4/ZnWO_4$	Solar light	-	-	98	70	O_2^-, ȮH	Reddy et al., 2020
Ciprofloxacin	Fe_3O_4@ $NiFe_2O_4$/Phosphorus-doped g-C_3N_4	Solar light	20 mg/L	-	90	60	ȮH	Mishra et al., 2020
Sodium dodecyl benzene sulfonate	$NiFe_2O_4$/sepiolite	Microwave radiation	21.0 μmol/L	3.2 g/L	100	01	O_2^-, ȮH, holes	(Shen et al., 2018)
Azo fuchsine	$NiFe_2O_4$/sepiolite	Microwave radiation	21.0 μmol/L	3.2 g/L	100	05	O_2^-, ȮH, holes	Shen et al., 2018
Methyl parathion	$NiFe_2O_4$/sepiolite	Microwave radiation	21.0 μmol/L	3.2 g/L	100	03	O_2^-, ȮH, holes	Shen et al., 2018
Crystal violet	$NiFe_2O_4$/sepiolite	Microwave radiation	21.0 μmol/L	3.2 g/L	100	06	O_2^-, ȮH, holes	Shen et al., 2018
Azo fuchsine	$NiFe_2O_4$/diatomite	Microwave radiation	21.0 μmol/L	3.2 g/L	90.5	05	O_2^-, ȮH, holes	Shen et al., 2018
Azo fuchsine	$NiFe_2O_4$/kaolinite	Microwave radiation	21.0 μmol/L	3.2 g/L	68.2	05	O_2^-, ȮH, holes	Shen et al., 2018
MB	$NiFe_2O_4$@GO	UV light	0.04 mM	0.5 mg/L	100	120	ȮH, holes	(Bayantong et al., 2020)
MB	$BiVO_4/NiFe_2O_4$	Natural sunlight	40 mL	40 mg	95	240	ȮH	(Sakhare et al., 2020)
MB	$BiVO_4/NiFe_2O_4$	Collected sunlight	40 mL	40 mg	98	30	ȮH	Sakhare et al., 2020
MB	Zeolitic imidazolate framework-8/$NiFe_2O_4$	Halogen lamp	10 mg/L	50 mg	94	120	-	(Faraji et al., 2021)
MB	$NiFe_2O_4$/MXene	-	-	-	74	70	ȮH, $O_2^{\cdot}$	(Rasheed et al., 2021)
MB	$ZnS/NiFe_2O_4$	Sunlight	100 mL of 20 mg/L	5 mg	93	120	ȮH, O_2^-	Dharmaraja et al., 2021
RB	$ZnS/NiFe_2O_4$	Sunlight	100 mL of 20 mg/L	5 mg	72	120	ȮH, O_2^-	Dharmaraja et al., 2021
TC	Sulphur-doped carbon nitride/$NiFe_2O_4$	LED visible light	-	-	97	60	ȮH	(Palanivel and Alagiri, 2020)
MB	Pectin/$NiFe_2O_4$	Visible light	0.05 mM	0.5 g/L	99.57	35	ȮH	(Gupta et al., 2020)
Remazol black 5	Pectin/$NiFe_2O_4$	Visible light	0.05 mM	0.5 g/L	99.68	30	ȮH	Gupta et al., 2020
TC	g-$C_3N_4/NiFe_2O_4$/Ag	Visible light	30 mL of 20 mg/L	20 mg	92.1	120	ȮH, O_2^-	(Hassanzadeh-Tabrizi, 2021)
Metronidazole	$NiFe_2O_4$/chitosan/BiOI	Simulated sunlight	20 mg/L	0.04 g/L	100	200	ȮH, O_2^-	Sadat et al., 2021
RB	$NiFe_2O_4$@hydroxyapatite-Sn^{2+}	Solar light	50 mL of 10 ppm	50 mg	99.2	40	ȮH, ȮOH, O_2^-, holes	(Ch et al., 2021)
Malachite green	$rGO/NiFe_2O_4$	Visible light	100 mL of 5×10^{-5} M	20 mg	96.5	120	O_2^-, ȮH, holes	(Tamilselvi et al., 2021)
TC	$NiFe_2O_4/BiPO_4$	Solar light	50 mL of 40 mg/L	15 mg	98	100	O_2^-, ȮH	(Koutavarapu et al., 2021)
RB	$NiFe_2O_4/BiPO_4$	Solar light	100 mg/L	15 mg	99	60	O_2^-, ȮH	(Koutavarapu et al., 2021)
Doxycycline	$NiFe_2O_4$/MWCNTs/BiOI	UV light	45 mg/L	1.25 g/L	92.18	150	O_2^-, holes	(Yan et al., 2021)
Acid red 14	$NiFe_2O_4$-mixed metal oxides	Visible light	100 mL of 20 mg/L	0.01 g	100	165	O_2^-, ȮH	(Veisi et al., 2021)
TC	$NiFe_2O_4$-$ZnWO_4$	Solar light	50 mL	15 mg	97.9	120	O_2^-, ȮH	(Koutavarapu et al., 2022)
MB	$NiFe_2O_4$-$ZnWO_4$	Solar light	50 mL	15 mg	99.6	60	O_2^-, ȮH	Koutavarapu et al., 2022
MB	$NiFe_2O_4$-$BiVO_4$	Sunlight	250 mL of 10 ppm	0.25 g	80	180	-	(Remlalfaka et al., 2021)
TC	$NiFe_2O_4/Bi_2WO_6$	Visible light	-	0.30 mg/mL	96.81	96	O_2^-, ȮH	Koutavarapu et al., 2021
MB	$NiFe_2O_4/Bi_2WO_6$	Visible light	-	0.30 mg/mL	99.16	60	O_2^-, ȮH	Koutavarapu et al., 2021
Paracetamol	F@g-$C_3N_4/NiFe_2O_4$	Visible light	25 mg/L	1 mg/mL	100	60	ȮH	(Palanivel et al., 2021)
RB	$rGO/NiFe_2O_4$/g-C_3N_4	Direct sunlight	-	-	100	40	ȮH	(Palanivel et al., 2020)
RB	$rGO/NiFe_2O_4$/g-C_3N_4	LED light	-	-	99	60	ȮH	Palanivel and Alagiri, 2020

which were adsorbed to the catalytic surface became non-harmful products through performing a chemical reaction with the active species (Chen and Liu, 2017).

Table 2 shows the types of $NiFe_2O_4$-based nanocomposites used to degrade the organic pollutant from the polluted water.

5. Recovery and reusability

Commonly, the sustainable methods to get back the used photocatalytic materials after the organic compound degradation are centrifugation and filtration, but these processes are limited because of their high time-consuming and cost of operation. Thus, a simple and faster approach to recovering the materials can be achieved using an external magnetic field. Based on this attempt, a one-time synthesized material can register in consecutive degradation reactions that have become beneficial and essential for the commercialized industries. Hence, the recover and reuse (3 to 4 times) nature of the photocatalyst with the effective percentage of degradation created a footprint to manage the contaminated water resources in a fulfilling way (Table 2).

6. Conclusion and future research expectations

The global challenge which all living creatures have to face in their lifetime is water pollution. Enormous technical methods have been taking part in the remedial activity of water for purification. In most cases, the method adopted depends upon the type of pollutant available in the adulterated water. Herein, we have discussed the performance of $NiFe_2O_4$-based nanocomposites, in particular binary $NiFe_2O_4$-based and ternary $NiFe_2O_4$-based composites on the road to water treatment as a photocatalyst, with conceivable explanation. Using these nanocomposites, namely organic pollutants (MO, MB, RB, CR, phenol, antibiotics, and so on), is more feasible, and most of the nanocomposites are magnetically recyclable with high stability. The reuse of photocatalyst in the repeated cycle creates further support for the degradation process. The adsorption capability of $NiFe_2O_4$ finds its way in the field of adsorption processes, although in order to enhance its photocatalytic activity, the authors made a decision that the $NiFe_2O_4$ should have collaboration with one or more semiconducting materials to form nanocomposites. They succeeded in these kinds of preparation, and the role of $NiFe_2O_4$-based nanocomposites as a catalyst, mainly in the dye degradation, shaped the contaminated water resources into the utmost purest form.

Our future researchers would benefit from clarifying and researching the following questions. Thus, (i) from this literature review, we can understand that, in some cases, the complete participation of unaccompanied $NiFe_2O_4$-based composites performed well in the degradation of organic pollutants. In other cases, a collaboration is required to carry out the degradation process with the assistance of supporting agents or conditions. Accordingly, the process of degradation depends on several parameters like pH of the solution, H_2O_2 concentration, $NaBH_4$ concentration, initial pollutant concentration, source of light, and temperature. However, there was no methodical comparison between these composites and their supporting agents. Thus, the researchers should develop any logical reason to prove the observed relationship. (ii) According to the published literature, researchers have reported the degradation of various pollutants using $NiFe_2O_4$-based composites. In spite of this, not much research study has focused on the degradation of substituted phenols (nitrophenol, chlorophenol), pesticides, pharmaceuticals, and personal care products. Therefore, it is very crucial to have deep and keen research using these composites for the above-mentioned pollutants. (iii) There are some reports in which complete degradation of pollutants has not been achieved using these composites. Furthermore, it may create an extra toxic co-pollutant spreading into our ecosystem, so future societies will need to overcome this downside. (iv) We cannot neglect the consumption of chemicals completely since their usage is increasing day by day in this scientific world. As a result, the consumed chemicals become an environmental threat to society. Therefore, more efforts have to be made for the upcoming development of photocatalysts to be born with superior efficiency to destroy organic contaminants within a short span of time and with less toxicity.

Funding inforamtion

There is no funding information available for this article.

Declaration of Competing Interest

The authors declare the following financial interests/personal relationships which may be considered as potential competing interests.

References

Adeleke, J.T., Theivasanthi, T., Thiruppathi, M., Swaminathan, M., Akomolafe, T., Alabi, A.B., 2018. Photocatalytic degradation of methylene blue by ZnO/$NiFe_2O_4$ nanoparticles. Appl. Surf. Sci. 455, 195–200. doi:10.1016/j.apsusc.2018.05.184.

Ahmad, M., Tamoor, M., Mustafa, G.M., Ishaq, S., Naseem, S., Murtaza, G., Kanwal, F., Atiq, S., 2020. Polymer based nickel ferrite as dielectric composite for energy storage applications. Synth. Met. 268, 1–9. doi:10.1016/j.synthmet.2020.116507.

Al, H., Tohamy, A., 2020. Optimization and adsorption behavior of nanostructured $NiFe_2O_4$/poly AMPS grafted biopolymer. J. Polym. Environ. doi:10.1007/s10924-020-01774-z.

Allafchian, A., Amir, S., Jalali, H., Bahramian, H., Ahmadvand, H., 2015. Preparation, characterization, and antibacterial activity of $NiFe_2O_4$/PAMA/Ag–TiO_2 nanocomposite. J. Magn. Magn. Mater. doi:10.1016/j.jmmm.2015.12.015.

Amiri, M., Eskandari, K., Salavati-Niasari, M., 2019. Magnetically retrievable ferrite nanoparticles in the catalysis application. Adv. Colloid Interface Sci. 271. doi:10.1016/j.cis.2019.07.003.

Ansari, F., Bazarganipour, M., Salavati-niasari, M., 2016. Materials science in semiconductor processing $NiTiO_3$/$NiFe_2O_4$ nanocomposites : Simple sol – gel autocombustion synthesis and characterization by utilizing onion extract as a novel fuel and green capping agent. Mater. Sci. Semicond. Process. 43, 34–40. doi:10.1016/j.mssp.2015.11.014.

Atacan, K., Güy, N., Çakar, S., Özacar, M., 2019. Efficiency of glucose oxidase immobilized on tannin modified $NiFe_2O_4$ nanoparticles on decolorization of dye in the Fenton and photo-biocatalytic processes. J. Photochem. Photobiol. A Chem. 382, 111935. doi:10.1016/j.jphotochem.2019.111935.

Babu, B., Koutavarapu, R., Shim, J., Yoo, K., 2020. Materials science in semiconductor processing SnO_2 quantum dots decorated $NiFe_2O_4$ nanoplates: 0D/2D heterojunction for enhanced visible-light-driven photocatalysis. Mater. Sci. Semicond. Process. 107, 104834. doi:10.1016/j.mssp.2019.104834.

Bagher, M., Salarizadeh, P., 2020. ScienceDirect Binary nickel ferrite oxide ($NiFe_2O_4$) nanoparticles coated on reduced graphene oxide as stable and high-performance asymmetric supercapacitor electrode material. Int. J. Hydrogen Energy. doi:10.1016/j.ijhydene.2020.07.063.

Bayantong, A.R.B., Shih, Y., Dong, C., Garcia-segura, S., De Luna, M.D.G., 2020. Nickel ferrite nanoenabled graphene oxide ($NiFe_2O_4$@GO) as photoactive nanocomposites for water treatment. Environ. Sci. Pollut. Res.. https://doi.org/10.1007/s11356-020-10545-1.

Bazgir, A., Khorshidi, A., Kamani, H., Ashrafi, S.D., 2019. Modeling of azo dyes adsorption on magnetic $NiFe_2O_4$/RGO nanocomposite using response surface methodology. J. Environ. Health Sci. Eng.. https://doi.org/10.1007/s40201-019-00409-3.

Bharadwaj, P.S.J., Gannavarapu, K.P., Kollipara, V.S., Dandamudi, R.B., 2021. Study of magneto-supercapacitance properties of nickel cobalt ferrite-activated carbon composite. J. Energy Storage. 36, 102444. doi:10.1016/j.est.2021.102444.

Borhan, A.I., Gherca, D., Iordan, A.R., 2019. One-pot synthesis of hierarchical magnetic porous-Fe_2O_3@$NiFe_2O_4$ composite with solid-phase morphology changes promoted by adsorption of anionic azo-dye. Mater. Res. Bull., 110664 doi:10.1016/j.materresbull.2019.110664.

Boychuk, V., Kotsyubynsky, V., Bandura, K., Fedorchenko, S., 2018. Nickel-Iron Spinel/Reduced Graphene Oxide Nanocomposites: Structural and Mossbauer Studies. IEEE 1–6. https://doi.org/10.1109/NAP.2018.8915082.

Boychuk, V., Kotsyubynsky, V., Bandura, K., Yaremiy, I., Zapukhlyak, R., Fedorchenko, S., 2019. Self-combustion synthesized $NiFe_2O_4$/reduced graphene oxide composite nanomaterials: Effect of chelating agent type on the crystal structure and magnetic properties. Mater. Today Proc. doi:10.1016/j.matpr.2019.10.026.

Brillas, E., Martínez-Huitle, C.A., 2015. Decontamination of wastewaters containing synthetic organic dyes by electrochemical methods. An updated review. Appl. Catal. B Environ. 166–167, 603–643. doi:10.1016/j.apcatb.2014.11.016.

Cao, H.L., Cai, F.Y., Yu, K., Zhang, Y.Q., Lü, J., Cao, R., 2019. Photocatalytic degradation of tetracycline antibiotics over CdS/nitrogen-doped-carbon composites derived from in situ carbonization of metal-organic frameworks. ACS Sustain. Chem. Eng. 7, 10847–10854. doi:10.1021/acssuschemeng.9b01685.

Ch, K., Dhar, S.S., Thakurata, D.G., Das, J., 2021. Sn (II) inserted on hydroxyapatite encapsulated nickel ferrite ($NiFe_2O_4$@HAp-Sn^{2+}): a novel nanocomposite for the effective photo- degradation of rhodamine B dye. J. Clean. Prod. 290, 125172. doi:10.1016/j.jclepro.2020.125172.

Chen, Y., Liu, K., 2017. SC. J. Alloys Compd doi:10.1016/j.jallcom.2016.12.153.

Chen, Y., Liu, K., 2017. SC. Powder Technol doi:10.1016/j.powtec.2017.03.005.
Chen, Y., Liu, K., 2017. A facile sol-gel method for the fabrication of nitrogen doped TiO_2/$NiFe_2O_4$/diatomite composite with enhanced photoactivity. Adv. Powder Technol. 2–8. doi:10.1016/j.apt.2017.06.003.
Chen, Y., Zhu, P., Duan, M., Li, J., Ren, Z., Wang, P., 2019. Applied Surface Science Fabrication of a magnetically separable and dual Z-scheme PANI/Ag_3PO_4/$NiFe_2O_4$ composite with enhanced visible-light photocatalytic activity for organic pollutant elimination. Appl. Surf. Sci. 486, 198–211. doi:10.1016/j.apsusc.2019.04.232.
Cui, H., Huang, X., Yu, Z., Chen, P., Cao, X., 2020. Application progress of enhanced coagulation in water treatment. RSC Adv. 10, 20231–20244. doi:10.1039/d0ra02979c.
Darwish, A.A.A., Rashad, M., AL-Aoh, H.A., 2019. Methyl orange adsorption comparison on nanoparticles: isotherm, kinetics, and thermodynamic studies. Dye. Pigment. 160, 563–571. doi:10.1016/j.dyepig.2018.08.045.
Dharmaraja, C., Nicholas, P.E., Ramya, P., Premkumar, I.J.I., Vijayan, V., Senthilkumar, N., 2021. Investigation on photocatalytic activity of ZnS/$NiFe_2O_4$ NCs under sunlight irradiation via a novel two-step synthesis approach. Inorg. Chem. Commun. 126, 108481. doi:10.1016/j.inoche.2021.108481.
Dutt, M.A., Hanif, M.A., Nadeem, F., Bhatti, H.N., 2020. A review of advances in engineered composite materials popular for wastewater treatment. J. Environ. Chem. Eng. 8, 104073. doi:10.1016/j.jece.2020.104073.
El-Sayyad, G.S., Abd Elkodous, M., El-Khawaga, A.M., Elsayed, M.A., El-Batal, A.I., Gobara, M., 2020. Merits of photocatalytic and antimicrobial applications of gamma-irradiated $Co_xNi_{1-x}Fe_2O_4$/SiO_2/TiO_2; X = 0.9 nanocomposite for pyridine removal and pathogenic bacteria/fungi disinfection: Implication for wastewater treatment. RSC Adv 10, 5241–5259. doi:10.1039/c9ra10505k.
Ensafi, A.A., Rezaei, B., 2019. Nickel-ferrite oxide decorated on reduced graphene oxide, an efficient and selective electrochemical sensor for detection of furazolidone. IEEE Sens. J. PP 1. doi:10.1109/JSEN.2019.2908994.
Faraji, A., Mehrdadi, N., Mohammad, N., Baghdadi, M., 2021. Enhanced photocatalytic activity by synergic action of ZIF-8 and $NiFe_2O_4$ under visible light irradiation. J. Mol. Struct. 1223. https://doi.org/10.1016/j.molstruc.2020.129028.
Foletto, E.L., Dotto, G.L., 2019. Preparation and characterization of $NiFe_2O_4$/activated carbon composite as potential magnetic adsorbent for removal of ibuprofen and ketoprofen pharmaceuticals from aqueous solutions. J. Clean. Prod. 229, 828–837. https://doi.org/10.1016/j.jclepro.2019.05.037.
Gautam, S., Shandilya, P., Singh, V.P., Raizada, P., Singh, P., 2016. Solar photocatalytic mineralization of antibiotics using magnetically separable $NiFe_2O_4$ supported onto graphene sand composite and bentonite. J. Water Process Eng. 14, 86–100. doi:10.1016/j.jwpe.2016.10.008.
Ge, M., Hu, Z., 2016. Novel magnetic AgBr/$NiFe_2O_4$ composite with enhanced visible light photocatalytic performance. Ceram. Int. doi:10.1016/j.ceramint.2016.01.035.
Ge, M., Liu, W., Hu, X., Li, Z., 2017. Magnetically separable Ag/AgBr/$NiFe_2O_4$ composite as a highly efficient visible light plasmonic photocatalyst. J. Phys. Chem. Solids. 109, 1–8. doi:10.1016/j.jpcs.2017.05.008.
Gebreslassie, G., Bharali, P., Chandra, U., Sergawie, A., 2019. Novel g-C_3N_4/graphene/$NiFe_2O_4$ nanocomposites as magnetically separable visible light driven photocatalysts. J. Photochem. Photobiol. A Chem. 382, 111960. doi:10.1016/j.jphotochem.2019.111960.
Gebreslassie, G., Bharali, P., Chandra, U., Sergawie, A.. Hydrothermal synthesis of g-C3N4/$NiFe_2O_4$ nanocomposite and its enhanced photocatalytic activity.
Gebreslassie, G., Bharali, P., Chandra, U., Sergawie, A., 2019. Journal of photochemistry & photobiology A: chemistry novel g-C_3N_4/graphene/$NiFe_2O_4$ nanocomposites as magnetically separable visible light driven photocatalysts. J. Photochem. Photobiol. A Chem. 382, 111960. doi:10.1016/j.jphotochem.2019.111960.
Gor, A.H., Dave, P.N., 2019. Adsorptive abatement of ciprofloxacin using $NiFe_2O_4$ and thermodynamic studies. Polym. Bull. doi:10.1007/s00289-019-03032-2.
Gorgizadeh, M., Azarpira, N., Lot, M., Daneshvar, F., Salehi, F., Sattarahmady, N., 2019. Sonodynamic cancer therapy by a nickel ferrite/carbon nanocomposite on melanoma tumor: In vitro and in vivo studies. Photodiagnosis Photodyn Ther 27, 27–33. https://doi.org/10.1016/j.pdpdt.2019.05.023.
Gorgizadeh, M., Azarpira, N., Sattarahmady, N., 2018. Colloids and surfaces B: biointerfaces in vitro and in vivo tumor annihilation by near-infrared photothermal effect of a $NiFe_2O_4$/C nanocomposite. Colloid. Surface. B Biointerface. 170, 393–400. doi:10.1016/j.colsurfb.2018.06.034.
Gupta, K., Dawra, K., Dhamija, N., Tikoo, K., Kumar, V., Bansal, S., Sharma, A., Singhal, S., 2020. Synchronous role of coupled adsorption and photocatalytic oxidation on hybrid nanomaterials of pectin and nickel ferrite generating excellent removal efficiency for toxic dye effluents. New J. Chem. doi:10.1039/D0NJ01414A.
Gupta, K., Kaushik, A., Tikoo, K.B., Kumar, V., Singhal, S., 2017. Enhanced Catalytic Activity of Composites of $NiFe_2O_4$ and Nano Cellulose Derived from Waste Biomass for the Mitigation of Organic Pollutants. King Saud University doi:10.1016/j.arabjc.2017.07.016.
Gusain, R., Gupta, K., Joshi, P., Khatri, O.P., 2019. Adsorptive removal and photocatalytic degradation of organic pollutants using metal oxides and their composites: a comprehensive review. Adv. Colloid Interface Sci. 272, 102009. doi:10.1016/j.cis.2019.102009.
Hansima, M.A.C.K., Makehelwala, M., Jinadasa, K.B.S.N., Wei, Y., Nanayakkara, K.G.N., Herath, A.C., Weerasooriya, R., 2021. Fouling of ion exchange membranes used in the electrodialysis reversal advanced water treatment: a review. Chemosphere 263, 127951. doi:10.1016/j.chemosphere.2020.127951.
Hassan, N.S., Jalil, A.A., 2022. A review on self-modification of zirconium dioxide nanocatalysts with enhanced visible-light-driven photodegradation of organic pollutants. J. Hazard. Mater. 423, 126996. doi:10.1016/j.jhazmat.2021.126996.
Hassanzadeh-Tabrizi, S.A., 2021. Synthesis of $NiFe_2O_4$/Ag nanoparticles immobilized on mesoporous g-C_3N_4 sheets and application for degradation of antibiotics. J. Photochem. Photobiol. A Chem. 418, 113398. doi:10.1016/j.jphotochem.2021.113398.
He, Z., Xia, Y., Su, J., Tang, B., 2019. Fabrication of magnetically separable $NiFe_2O_4$/$Bi_{24}O_{31}Br_{10}$ nanocomposites and excellent photocatalytic performance under visible light irradiation. Opt. Mater. (Amst). 88, 195–203. doi:10.1016/j.optmat.2018.11.025.
Hezam, F.A., Nur, O., Mustafa, M.A., 2020. Synthesis, structural, optical and magnetic properties of $NiFe_2O_4$/MWCNTs/ZnO hybrid nanocomposite for solar radiation driven photocatalytic degradation and magnetic separation. Colloid. Surface. A 592, 124586. doi:10.1016/j.colsurfa.2020.124586.
Hezam, F.A., Rajeh, A., Nur, O., Mustafa, M.A., 2020. Synthesis and physical properties of spinel ferrites/MWCNTs hybrids nanocomposites for energy storage and photocatalytic applications. Phys. B Phys. Condens. Matter., 412389 doi:10.1016/j.physb.2020.412389.
Hussain, D., Siddiqui, M.F., 2020. Preparation of $NiFe_2O_4$/polythiophene nanocomposite and its enhanced adsorptive uptake of Janus green B and Fuchsin basic from aqueous solution: Isotherm and kinetics studies. Environ. Prog. Sustain. Energy 1–11. https://doi.org/10.1002/ep.13371.
Iftikhar, S., Farooq, M., Haider, S., Musaddiq, S., Shakir, I., Shahid, M., 2019. The impact of carbon nanotubes on the optical, electrical, and magnetic parameters of Ni^{2+} and Co^{2+} based spinel ferrites. Ceram. Int. 45, 21150–21161. doi:10.1016/j.ceramint.2019.07.092.
Inyinbor, A.A., Adekola, F.A., Olatunji, G.A., 2016. Kinetics, isotherms and thermodynamic modeling of liquid phase adsorption of Rhodamine B dye onto Raphia hookerie fruit epicarp. Water Resour. Ind. 15, 14–27. doi:10.1016/j.wri.2016.06.001.
Ismael, M., 2021. Ferrites as solar photocatalytic materials and their activities in solar energy conversion and environmental protection: a review. Sol. Energy Mater. Sol. Cells. 219, 110786. doi:10.1016/j.solmat.2020.110786.
Jabar, J.M., Odusote, Y.A., Alabi, K.A., Ahmed, I.B., 2020. Kinetics and mechanisms of congo-red dye removal from aqueous solution using activated Moringa oleifera seed coat as adsorbent. Appl. Water Sci. 10, 1–11. doi:10.1007/s13201-020-01221-3.
Janani, B., Syed, A., Sruthi, L., Sivaranjani, P.R., Elgorban, A.M., Bahkali, A.H., Zaghloul, N.S.S., Badawy, M.M., Das, A., Khan, S.S., 2021. Visible light driven photocatalytic activity and efficient antibacterial activity of $ZnFe_2O_4$ decorated CdO nanohybrid heterostructures synthesized by ultrasonic-assisted method. Colloid. Surface. A Physicochem. Eng. Asp. 628, 127307. doi:10.1016/j.colsurfa.2021.127307.
Jawad, A.H., Ngoh, Y.S., Radzun, K.A., 2018. Utilization of watermelon (Citrullus lanatus) rinds as a natural low-cost biosorbent for adsorption of methylene blue: kinetic, equilibrium and thermodynamic studies. J. Taibah Univ. Sci. 12, 371–381. doi:10.1080/16583655.2018.1476206.
Jawad, A.H., Rashid, R.A., Ishak, M.A.M., Ismail, K., 2018. Adsorptive removal of methylene blue by chemically treated cellulosic waste banana (Musa sapientum) peels. J. Taibah Univ. Sci. 12, 809–819. doi:10.1080/16583655.2018.1519893.
Jawad, A.H., Sabar, S., Ishak, M.A.M., Wilson, L.D., Ahmad Norrahma, S.S., Talari, M.K., Farhan, A.M., 2017. Microwave-assisted preparation of mesoporous-activated carbon from coconut (Cocos nucifera) leaf by H_3PO_4 activation for methylene blue adsorption. Chem. Eng. Commun. 204, 1143–1156. doi:10.1080/00986445.2017.1347565.
Kamal, S., Balu, S., Palanisamy, S., Uma, K., Velusamy, V., Yang, T.C.K., 2019. Synthesis of boron doped C_3N_4/$NiFe_2O_4$ nanocomposite: An enhanced visible light photocatalyst for the degradation of methylene blue. Results Phys 12, 1238–1244. doi:10.1016/j.rinp.2019.01.004.
Katowah, D.F., Hussein, M.A., Alam, M.M., Ismail, S.H., Osman, O.I., Sobahi, T.R., Asiri, A.M., Ahmed, J., Rahman, M.M., 2020. Designed network of ternary core-shell PPCOT/$NiFe_2O_4$/C-SWCNTs nanocomposites. A Selective Fe^{3+} ionic sensor. J. Alloys Compd. 834, 155020. doi:10.1016/j.jallcom.2020.155020.
Kefeni, K.K., Mamba, B.B., 2020. Photocatalytic application of spinel ferrite nanoparticles and nanocomposites in wastewater treatment: review. Sustain. Mater. Technol. 23, e00140. doi:10.1016/j.susmat.2019.e00140.
Kefeni, K.K., Mamba, B.B., Msagati, T.A.M., 2017. Application of spinel ferrite nanoparticles in water and wastewater treatment: a review. Sep. Purif. Technol. 188, 399–422. doi:10.1016/j.seppur.2017.07.015.
Kefeni, K.K., Msagati, T.A.M., Nkambule, T.T.I., Mamba, B.B., 2019. Spinel ferrite nanoparticles and nanocomposites for biomedical applications and their toxicity. Mater. Sci. Eng. C., 110314 doi:10.1016/j.msec.2019.110314.
Khorshidi, P., 2020. Adsorptive removal of mercury (II), copper (II), and lead (II) ions from aqueous solutions using glutathionefunctionalized $NiFe_2O_4$/graphene oxide composite. Res. Chem. Intermed.. https://doi.org/10.1007/s11164-020-04164-1.
Khosroshahi, Negin, Bakhtian, Mahnaz, Safarifard, Vahid, 2022. Mechanochemical synthesis of ferrite/MOF nanocomposite: Efficient photocatalyst for the removal of meropenem and hexavalent chromium from water. J. Photochem. Photobiol. 114033, 431. doi:10.1016/j.jphotochem.2022.114033.
Kirankumar, V.S., Sumathi, S., 2020. A review on photodegradation of organic pollutants using spinel oxide. Mater. Today Chem. 18, 100355. doi:10.1016/j.mtchem.2020.100355.
Koe, W.S., Lee, J.W., Chong, W.C., 2019. An overview of photocatalytic degradation: photocatalysts, mechanisms, and development of photocatalytic membrane. Colloid Interface Sci. J. doi:10.1007/s11356-019-07193-5.
Koutavarapu, R., Rao, M., Lee, S., Rao, M.C., Lee, Y., Shim, J., 2021. Synthesis of 2D $NiFe_2O_4$ nanoplates/2D Bi_2WO_6 nanoflakes heterostructure: An enhanced Z-scheme charge transfer and separation for visible-light-driven photocatalytic degradation of toxic pollutants. J. Environ. Chem. Eng. 9, 105893. doi:10.1016/j.jece.2021.105893.
Koutavarapu, R., Tamtam, M.R., Myla, C.R., Cho, M., Shim, J., 2021. Enhanced solar-light-driven photocatalytic properties of novel Z-scheme binary $BiPO_4$ nanorods anchored onto $NiFe_2O_4$ nanoplates: efficient removal of toxic organic pollutants. J. Environ. Sci. 102, 326–340. doi:10.1016/j.jes.2020.09.021.
Koutavarapu, R., Venkata, C., Syed, K., Raghava, K., Saleh, T.A., Lee, D., Shim, J., Aminabhavi, T.M., 2022. Novel Z-scheme binary zinc tungsten oxide/nickel ferrite nanohy-

brids for photocatalytic reduction of chromium (Cr(VI)), photoelectrochemical water splitting and degradation of toxic organic pollutants. J. Hazard. Mater. 423, 127044. doi:10.1016/j.jhazmat.2021.127044.
Kumar, A., Singh, A.K., Tomar, M., Gupta, V., Kumar, P., Singh, K., 2020. Electromagnetic interference shielding performance of lightweight $NiFe_2O_4$/rGO nanocomposite in X-band frequency range. Ceram. Int. 0–1. doi:10.1016/j.ceramint.2020.03.092.
Kumar, M., Singh, H., Singh, H., 2019. Biopolymer modified transition metal spinel ferrites for removal of fluoride ions from water. Environ. Nanotechnology, Monit. Manag. 12, 100237. doi:10.1016/j.enmm.2019.100237.
Kumar, N., Kumar, A., Huang, G., Wu, W., Tseng, T.Y., 2017. Facile synthesis of mesoporous $NiFe_2O_4$/CNTs nanocomposite cathode material for high performance asymmetric pseudocapacitors. Appl. Surf. Sci. doi:10.1016/j.apsusc.2017.10.095.
Kumar, P.A., Laxma, P.V., Kwon, E., Kim, K., Akter, T., Kalagara, S., 2016. Recent advances in photocatalytic treatment of pollutants in aqueous media. Environ. Int. 91, 94–103. doi:10.1016/j.envint.2016.02.012.
Lashkenari, M.S., Ghorbani, M., Naghibi, H., 2019. Synthesis and characterization of polyrhodanine/nickel ferrite nanocomposite with an effective and broad spectrum antibacterial activity. Polym. Technol. Mater. 00, 1–10. doi:10.1080/25740881.2018.1563124.
Li, X., Wang, L., Zhang, L., Zhuo, S., 2017. A facile route to the synthesis of magnetically separable BiOBr/$NiFe_2O_4$ composites with enhanced photocatalytic performance. Appl. Surf. Sci. doi:10.1016/j.apsusc.2017.05.013.
Li, X., Xu, H., Wang, L., Zhang, L., Cao, X., Guo, Y., 2018. Spinel $NiFe_2O_4$ nanoparticles decorated BiOBr nanosheets for improving the photocatalytic degradation of organic dye pollutants. J. Taiwan Inst. Chem. Eng. 0, 1–8. doi:10.1016/j.jtice.2018.01.043.
Li, Y., Zhang, Z., Pei, L., Li, X., Fan, T., Ji, J., Shen, J., Ye, M., 2016. Multifunctional photocatalytic performances of recyclable Pd-$NiFe_2O_4$/reduced graphene oxide nanocomposites via different co-catalyst strategy. Applied Catal. B, Environ. doi:10.1016/j.apcatb.2016.02.054.
Liang, J., Wei, Y., Zhang, J., Yao, Y., He, G., Tang, B., Chen, H., 2018. Scalable green method to fabricate magnetically separable $NiFe_2O_4$-Reduced Graphene Oxide nanocomposites with enhanced photocatalytic performance driven by visible light. Materials and Interfaces. https://doi.org/10.1021/acs.iecr.8b00218.
Liang, Y., He, Y., Zhang, Y., 2017. SC, Adsorption property of Alizarin Red S by $NiFe_2O_4$/polyaniline magnetic composite. Biochem. Pharmacol. doi:10.1016/j.jece.2017.12.022.
Lingamdinne, L.P., Choi, Y., Kim, I., Yang, J., Koduru, J.R., Chang, Y., 2016. Preparation and characterization of porous reduced graphene oxide based inverse spinel nickel ferrite nanocomposite for adsorption removal of radionuclides. J. Hazard. Mater. doi:10.1016/j.jhazmat.2016.12.035.
Liu, J., Wang, N., Zhang, H., Baeyens, J., 2019. Adsorption of Congo red dye on $Fe_xCo_{3-x}O_4$ nanoparticles. J. Environ. Manage. 238, 473–483. doi:10.1016/j.jenvman.2019.03.009.
Livani, M.J., Ghorbani, M., 2017. Fabrication of $NiFe_2O_4$ magnetic nanoparticles loaded on activated carbon as novel nanoadsorbent for Direct Red 31 and Direct Blue 78 adsorption. Environ 3330. https://doi.org/10.1080/09593330.2017.1370024.
Livani, M.J., Ghorbani, M., Mehdipour, H., 2018. Preparation of an activated carbon from hazelnut shells and its hybrids with magnetic $NiFe_2O_4$ nanoparticles. New Carbon Mater. 33, 578–586. doi:10.1016/S1872-5805(18)60358-0.
Mamba, G., Gangashe, G., Moss, L., Hariganesh, S., Thakur, S., Vadivel, S., Mishra, A.K., Vilakati, G.D., Muthuraj, V., Nkambule, T.T.I., 2020. State of the art on the photocatalytic applications of graphene based nanostructures: from elimination of hazardous pollutants to disinfection and fuel generation. J. Environ. Chem. Eng. 8, 103505. doi:10.1016/j.jece.2019.103505.
Masmali, N.A., Osman, Z., Arof, A.K., 2021. Recent developments in zinc-based two-cation oxide spinels: from synthesis to applications. Ceram. Int. 47, 2949–2962. doi:10.1016/j.ceramint.2020.09.249.
Masunga, O.K.Mmelesi, Kefeni, K.K., Mamba, B.B., 2019. Recent advances in copper ferrite nanoparticles and nanocomposites synthesis, magnetic properties and application in water treatment: review. J. Environ. Chem. Eng. 7, 103179. doi:10.1016/j.jece.2019.103179.
Meng, F., Xu, J., Dai, H., Yu, Y., Lin, D., 2022. Supporting information even incorporation of nitrogen into Fe^0 nanoparticles as crystalline Fe_4N for efficient and selective trichloroethylene degradation table of contents. Environ. Sci. Technol. 56 (7), 4489–4497. https://doi.org/10.1021/acs.est.1c08671.
Mishra, P., Behera, A., Kandi, D., Parida, K., 2019. Nanoscale Adv. 1864–1879. doi:10.1039/c9na00018f.
Mishra, P., Behera, A., Kandi, D., Ratha, S., Parida, K., 2020. Novel magnetic retrievable visible-light-driven ternary Fe_3O_4@$NiFe_2O_4$/phosphorus-doped g-C_3N_4 nanocomposite photocatalyst with significantly enhanced activity through a double-Z-scheme system. Inorg. Chem. 59, 4255–4272. doi:10.1021/acs.inorgchem.9b02996.
Mmelesi, O.K., Masunga, N., Kuvarega, A., Nkambule, T.T., Mamba, B.B., Kefeni, K.K., 2021. Cobalt ferrite nanoparticles and nanocomposites: photocatalytic, antimicrobial activity and toxicity in water treatment. Mater. Sci. Semicond. Process. 123, 105523. doi:10.1016/j.mssp.2020.105523.
Moghaddam, A.Z., Ghiamati, E., Pourashuri, A., Allahresani, A., 2018. Modified nickel ferrite nanocomposite/functionalized chitosan as a novel adsorbent for the removal of acidic dyes. Int. J. Biol. Macromol. 120, 1714–1725. doi:10.1016/j.ijbiomac.2018.09.198.
Mohammad, M.S., Ebrahimzadeh, A., Mortazavi-derazkola, A.N.S., 2020. Novel NiFe/Si/Au magnetic nanocatalyst : Biogenic synthesis, efficient and reusable catalyst with enhanced visible light photocatalytic degradation and antibacterial activity. Appl. Organomet. Chem. 1–12. https://doi.org/10.1002/aoc.5467.
Mondal, N.K., Kar, S., 2018. Potentiality of banana peel for removal of Congo red dye from aqueous solution: isotherm, kinetics and thermodynamics studies. Appl. Water Sci. 8, 1–12. doi:10.1007/s13201-018-0811-x.
Moradi, S., Taghavi, S., Ali, F., 2018. Green synthesis and characterization of magnetic $NiFe_2O_4$4@ZnO nanocomposite and its application for photocatalytic degradation of organic dyes. J. Mater. Sci. Mater. Electron. 0, 0. doi:10.1007/s10854-018-9548-4.
Mukherjee, A., Chakrabarty, S., Su, W., Basu, S., 2018. Nanostructured nickel ferrite embedded in reduced graphene oxide for electrocatalytic hydrogen evolution reaction. Mater. Today Energy. 8, 118–124. doi:10.1016/j.mtener.2018.03.004.
Muthu, K.S., Lakshminarasimhan, N., Perumal, P., 2017. One-pot synthesis of $LaFeO_3$-$NiFe_2O_4$ nanocomposite ceramic by egg- white method and its magnetic and dielectric properties. Solid State Sci. 72, 33–40. doi:10.1016/j.solidstatesciences.2017.08.002.
Muthusamy, A., Arunkumar, M., Kannapiran, N., 2017. Electrical and magnetic properties of poly (m-phenylenediamine)/$NiFe_2O_4$ nanocomposites. J. Mater. Sci. Mater. Electron. 0, 0. doi:10.1007/s10854-017-7468-3.
Nada, A.A., Nasr, M., Viter, R., Miele, P., Roualdes, S., Bechelany, M., 2017. Mesoporous $ZnFe_2O_4$@TiO_2 nanofibers prepared by electrospinning coupled to PECVD as highly performing photocatalytic materials. J. Phys. Chem. C. 121. doi:10.1021/acs.jpcc.7b08567.
Narang, S.B., Pubby, K., 2021. Nickel spinel ferrites: a review. J. Magn. Magn. Mater. 519, 167163. doi:10.1016/j.jmmm.2020.167163.
Nasiri, R., Arsalani, N., Panahian, Y., 2018. One-pot synthesis of novel magnetic three-dimensional graphene/chitosan/nickel ferrite nanocomposite for lead ions removal from aqueous solution: RSM modelling design. J. Clean. Prod. doi:10.1016/j.jclepro.2018.08.059.
Naushad, M., Ahamad, T., Al-maswari, B.M., Alqadami, A.A., Alshehri, S.M., 2017. Nickel ferrite bearing nitrogen-doped mesoporous carbon as efficient adsorbent for the removal of highly toxic metal ion from aqueous medium. Chem. Eng. J. doi:10.1016/j.cej.2017.08.079.
Nawaz, M., Shahzad, A., Tahir, K., Kim, J., Moztahida, M., Jang, J., Alam, M.B., Lee, S.H., Jung, H.Y., Lee, D.S., 2020. Photo-Fenton reaction for the degradation of sulfamethoxazole using a multi-walled carbon nanotube- $NiFe_2O_4$ composite. Chem. Eng. J. 382, 123053. doi:10.1016/j.cej.2019.123053.
Nivetha, R., Santhosh, C., Kollu, P., Jeong, S.K., 2017. Cobalt and nickel ferrites based graphene nanocomposites for electrochemical hydrogen evolution. J. Magn. Magn. Mater. doi:10.1016/j.jmmm.2017.05.083.
Online, V.A., Choi, Y., Kim, I., Chang, Y., Koduru, J.R., Yang, J.K., 2016. RSC Adv. doi:10.1039/C6RA10134H.
Online, V.A., Doebelin, N., Vanags, M., Smits, K., Kisand, V., 2016. RSC Adv. doi:10.1039/C6RA00728G.
Online, V.A., Song, T., Lv, M., Wang, T., Qin, J., Zeng, H., 2016. RSC Adv. doi:10.1039/C6RA08356K.
Oyekanmi, A.A., Ahmad, A., Hossain, K., Rafatullah, M., 2019. Statistical optimization for adsorption of Rhodamine B dye from aqueous solutions. J. Mol. Liq. 281, 48–58. doi:10.1016/j.molliq.2019.02.057.
Palanivel, B., Alagiri, M., 2020. Construction of rGO Supported Integrative $NiFe_2O_4$/g-C_3N_4 Nanocomposite: Role of Charge Transfer for Boosting the OH Radical Production to Enhance the Photo-Fenton Degradation. ChemistrySelect 9765–9775. https://doi.org/10.1002/slct.202002519.
Palanivel, B., Ayappan, C., Jayaraman, V., Chidambaram, S., Maheswaran, R., Mani, A., 2019. Materials Science in Semiconductor Processing Inverse spinel $NiFe_2O_4$ deposited g-C_3N_4 nanosheet for enhanced visible light photocatalytic activity. Mater. Sci. Semicond. Process. 100, 87–97. doi:10.1016/j.mssp.2019.04.040.
Palanivel, B., Hu, C., Shkir, M., Alfaify, S., Ibrahim, F.A., Hamdy, M.S., Mani, A., 2021. Fluorine doped g-C_3N_4 coupled $NiFe_2O_4$ heterojunction: Consumption of H_2O_2 for production of hydroxyl radicals towards paracetamol degradation. Colloid Interface Sci. Commun. 42, 100410. doi:10.1016/j.colcom.2021.100410.
Palanivel, B., Mani, A., 2020. Conversion of a Type-II to a Z Scheme Heterojunction by Intercalation of a 0D Electron Mediator between the Integrative $NiFe_2O_4$/gC_3N_4 Composite Nanoparticles: Boosting the Radical Production for Photo-Fenton Degradation. ACS Omega. https://doi.org/10.1021/acsomega.0c02477.
Palanivel, B., Shkir, M., Alshahrani, T., Mani, A., 2020. Novel $NiFe_2O_4$ deposited S-doped g-C_3N_4 nanorod: visible light-driven heterojunction for photo-Fenton like tetracycline degradation. Journal P of, Diam. Relat. Mater., 108148 doi:10.1016/j.diamond.2020.108148.
Pangarkar, B.L., Sane, M.G., Parjane, S.B., Guddad, M., 2014. Status of membrane distillation for water and wastewater treatment-a review. Desalin. Water Treat. 52, 5199–5218. doi:10.1080/19443994.2013.808422.
Park, C.M., Kim, Y.M., Kim, K.H., Wang, D., Su, C., Yoon, Y., 2019. Potential utility of graphene-based nano spinel ferrites as adsorbent and photocatalyst for removing organic/inorganic contaminants from aqueous solutions: a mini review. Chemosphere 221, 392–402. doi:10.1016/j.chemosphere.2019.01.063.
Paul, A., Dhar, S.S., 2019. Construction of hierarchical $MnMoO_4$/$NiFe_2O_4$ nanocomposite: Highly efficient visible light driven photocatalyst in the degradation of different polluting dyes in aqueous medium. Colloid. Surface. A Physicochem. Eng. Asp., 124090 doi:10.1016/j.colsurfa.2019.124090.
Pérez-González, A., Urtiaga, A.M., Ibáñez, R., Ortiz, I., 2012. State of the art and review on the treatment technologies of water reverse osmosis concentrates. Water Res 46, 267–283. doi:10.1016/j.watres.2011.10.046.
Ponnamma, D., Aljarod, O., Parangusan, H., Al-, M.A.A., 2019. Electrospun nanofibers of PVDF-HFP composites containing magnetic nickel ferrite for energy harvesting application. Mater. Chem. Phys. doi:10.1016/j.matchemphys.2019.122257.
Qin, H., He, Y., Xu, P., Huang, D., Wang, Z., Wang, H., Wang, Z., Zhao, Y., Tian, Q., Wang, C., 2021. Spinel ferrites (MFe_2O_4): Synthesis, improvement and catalytic application in environment and energy field. Adv. Colloid Interface Sci. 294, 102486. doi:10.1016/j.cis.2021.102486.
Rahman, A., Warsi, M.F., Shakir, I., Shahid, M., Zulfiqar, S., 2020. Fabrication of Ce^{3+} substituted nickel ferrite-reduced graphene oxide heterojunction with high pho-

tocatalytic activity under visible light irradiation. J. Hazard. Mater. 394, 1–18. doi:10.1016/j.jhazmat.2020.122593.

Rasheed, T., Rasheed, A., Munir, S., Ajmal, S., Muhammad, Z., Alsafari, I.A., Ragab, S.A., Agboola, P.O., Shakir, I., 2021. A cost-effective approach to synthesize $NiFe_2O_4$/MXene heterostructures for enhanced photodegradation performance and anti-bacterial activity. Adv. Powder Technol. 32, 2248–2257. doi:10.1016/j.apt.2021.05.006.

Reddy, C.V., Koutavarapu, R., Reddy, K.R., Shetti, N.P., Aminabhavi, T.M., Shim, J., 2020. Z-scheme binary 1D $ZnWO_4$ nanorods decorated 2D $NiFe_2O_4$ nanoplates as photocatalysts for high efficiency photocatalytic degradation of toxic organic pollutants from wastewater. J. Environ. Manage. 268, 110677. doi:10.1016/j.jenvman.2020.110677.

Remlalfaka, W., Murugesan, C., Anantharamaiah, P.N., Prabu, N.M., 2021. Fabrication of magnetically recoverable $BiVO_4$/$NiFe_2O_4$ composites for the photocatalytic degradation of methylene blue. Ceram. Int. 47, 11526–11535. doi:10.1016/j.ceramint.2020.12.281.

Rosal, R., Rodríguez, A., Perdigón-Melón, J.A., Petre, A., García-Calvo, E., Gómez, M.J., Agüera, A., Fernández-Alba, A.R., 2010. Occurrence of emerging pollutants in urban wastewater and their removal through biological treatment followed by ozonation. Water Res 44, 578–588. doi:10.1016/j.watres.2009.07.004.

Sadat, F., Al-musawi, T.J., Abu, G., Pelalak, R., Khataee, A., Nasseh, N., 2021. Photocatalytic performance of a nickel ferrite/chitosan/bismuth (III) oxyiodide nanocomposite for metronidazole degradation under simulated sunlight illumination. J. Environ. Chem. Eng. 9, 105619. doi:10.1016/j.jece.2021.105619.

Saffarzadeh, S., Nabiyouni, G., Ghanbari, D., 2016. Preparation of $Ni(OH)_2$, NiO and $NiFe_2O_4$ nanoparticles : magnetic and photo-catalyst $NiFe_2O_4$–NiO nanocomposites. J. Mater. Sci. Mater. Electron. doi:10.1007/s10854-016-5484-3.

Saffarzadeh, S., Nabiyouni, G., Heidary, F., 2019. A short time microwave method for synthesis of magnetic $NiFe_2O_4$/NiO nanocomposites as a clean technology in photocatalytic degradation of water pollutants. J. Mater. Sci. Mater. Electron. 0, 0. doi:10.1007/s10854-019-01132-3.

Sakhare, P.A., Pawar, S.S., Bhat, T.S., Yadav, S.D., Patil, G.R., Patil, P.S., Sheikh, A.D., 2020. Magnetically Recoverable $BiVO_4$/$NiFe_2O_4$Nanocomposite Photocatalyst For Efficient Detoxification of Polluted Water Under Collected Sunlight. Mater. Res. Bull. 129. https://doi.org/10.1016/j.materresbull.2020.110908.

Sandoval, C., Ranganathan, S., Ramírez, E., Mansilla, H.D., Dinamarca, R., Pecchi, G., Yáñez, J., 2019. Visible light assisted photodegradation of thimerosal by high performance $ZnFe_2O_4$/poly(o-phenylenediamine) composite. Mater. Res. Bull. 116, 8–15. doi:10.1016/j.materresbull.2019.04.008.

Scott, T., Zhao, H., Deng, W., Feng, X., Li, Y., 2019. Photocatalytic degradation of phenol in water under simulated sunlight by an ultrathin MgO coated Ag/TiO_2 nanocomposite. Chemosphere 216, 1–8. doi:10.1016/j.chemosphere.2018.10.083.

Shah, P., Joshi, K., Shah, M., et al., 2022. Photocatalytic dye degradation using nickel ferrite spinel and its nanocomposite. Environ. Sci. Pollut. Res. doi:10.1007/s11356-022-21248-0.

Sharifianjazi, F., Moradi, M., Parvin, N., Nemati, A., Jafari Rad, A., Sheysi, N., Abouchenari, A., Mohammadi, A., Karbasi, S., Ahmadi, Z., Esmaeilkhanian, A., Irani, M., Pakseresht, A., Sahmani, S., Shahedi Asl, M., 2020. Magnetic $CoFe_2O_4$ nanoparticles doped with metal ions: A review. Ceram. Int. 46, 18391–18412. doi:10.1016/j.ceramint.2020.04.202.

Shekari, H., Sayadi, M.H., Rezaei, M.R., Allahresani, A., PT, US CR, 2017. Surface. Interface. doi:10.1016/j.surfin.2017.06.006.

Shen, M., Fu, L., Tang, J., Liu, M., Song, Y., Tian, F., Zhao, Z., Zhang, Z., Dionysiou, D.D., 2018. Microwave hydrothermal-assisted preparation of novel spinel- $NiFe_2O_4$/natural mineral composites as microwave catalysts for degradation of aquatic organic pollutants. J. Hazard. Mater. 350, 1–9. doi:10.1016/j.jhazmat.2018.02.014.

Singh, C., Goyal, A., Bansal, S., Singhal, S., 2017. SiO_2@MFe_2O_4 core-shell nanostructures: Efficient photocatalysts with excellent dispersion properties. Mater. Res. Bull. 85, 109–120. https://doi.org/10.1016/j.materresbull.2016.09.010.

Singh, C., Goyal, A., Malik, R., Bansal, S., Singhal, S., 2017. Envisioning the attachment of CdS nanoparticles on the surface of MFe_2O_4(M = Zn, Co and Ni) nanocubes: analysis of structural, optical, magnetic and photocatalytic properties. J. Alloys Compd. 695, 351–363. doi:10.1016/j.jallcom.2016.10.198.

Singh, P., Sharma, K., Hasija, V., Sharma, V., Sharma, S., Raizada, P., Singh, M., Saini, A.K., Hosseini-Bandegharaei, A., Thakur, V.K., 2019. Systematic review on applicability of magnetic iron oxides–integrated photocatalysts for degradation of organic pollutants in water. Mater. Today Chem. 14, 100186. doi:10.1016/j.mtchem.2019.08.005.

Singh, P., Sonu, Raizada, P., Sudhaik, A., Shandilya, P., Thakur, P., Agarwal, S., Gupta, V.K., 2019. Enhanced photocatalytic activity and stability of AgBr/BiOBr/graphene heterojunction for phenol degradation under visible light. J. Saudi Chem. Soc. 23, 586–599. doi:10.1016/j.jscs.2018.10.005.

Sohrabnezhad, S., Rezaeimanesh, M., 2017. Synthesis and characterization of novel magnetically separable $NiFe_2O_4$@AlMCM-41-Cu_2O core-shell and its performance in removal of dye. Adv. Powder Technol. doi:10.1016/j.apt.2017.09.014.

Soleimani, M., Shahrokhi, B., 2018. ScienceDirect Polyrhodanine/$NiFe_2O_4$ nanocomposite: a novel electrocatalyst for hydrazine oxidation reaction. Int. J. Hydrogen Energy. 1–9. doi:10.1016/j.ijhydene.2018.05.019.

Sonu, V.Dutta, Sharma, S., Raizada, P., Hosseini-Bandegharaei, A., Kumar Gupta, V., Singh, P., 2019. Review on augmentation in photocatalytic activity of $CoFe_2O_4$ via heterojunction formation for photocatalysis of organic pollutants in water. J. Saudi Chem. Soc. 23, 1119–1136. doi:10.1016/j.jscs.2019.07.003.

Soufi, A., Hajjaoui, H., Elmoubarki, R., Abdennouri, M., Qourzal, S., Barka, N., 2021. Spinel ferrites nanoparticles: Synthesis methods and application in heterogeneous Fenton oxidation of organic pollutants – a review. Appl. Surf. Sci. Adv. 6, 100145. doi:10.1016/j.apsadv.2021.100145.

Sudhaik, A., Raizada, P., Shandilya, P., Singh, P., 2018. Magnetically recoverable graphitic carbon nitride and $NiFe_2O_4$ based magnetic photocatalyst for degradation of oxytetracycline antibiotic in simulated wastewater under solar light. J. Environ. Chem. Eng. 6, 3874–3883. doi:10.1016/j.jece.2018.05.039.

Suresh, R., Rajendran, S., Kumar, P.S., Vo, D.V.N., Cornejo-Ponce, L., 2021. Recent advancements of spinel ferrite based binary nanocomposite photocatalysts in wastewater treatment. Chemosphere 274, 129734. doi:10.1016/j.chemosphere.2021.129734.

Syed, A., Elgorban, A.M., Bahkali, A.H., Zaghloul, N.S.S., 2021. Coupling of nano-spinel $MgFe_2O_4$ on Co_3O_4 for heterogeneous photocatalysis and antibacterial applications: Insights of optoelectrical properties. Colloid. Interface Sci. Commun. 44, 100467. doi:10.1016/j.colcom.2021.100467.

Tamilselvi, R., Lekshmi, G.S., Padmanathan, N., Selvaraj, V., Bazaka, O., Levchenko, I., Bazaka, K., Mandhakini, M., 2021. $NiFe_2O_4$/rGO nanocomposites produced by soft bubble assembly for energy storage and environmental remediation, Journal P re of. Renew. Energy. doi:10.1016/j.renene.2021.07.088.

Thirupathy, C., Lims, S.C., Sundaram, S.J., Hossam, A., Kaviyarasu, K., 2020. Science Equilibrium synthesis and magnetic properties of $BaFe_{12}O_{19}$/$NiFe_2O_4$ nanocomposite prepared by co precipitation method. J. King Saud Univ. - Sci. 32, 1612–1618. doi:10.1016/j.jksus.2019.12.019.

Tian, N., Tian, X., Nie, Y., Yang, C., Zhou, Z., Li, Y., 2018. Biogenic manganese oxide: An efficient peroxymonosulfate activation catalyst for tetracycline and phenol degradation in water. Chem. Eng. J. 352, 469–476. doi:10.1016/j.cej.2018.07.061.

Tong, X., Zhao, L., Lin, X., Pan, X., Zhang, J., Duan, X., Li, Q., 2017. Electrochimica Acta High-index faceted nickel ferrite nanocrystals encapsulated by graphene with high performance for lithium-ion batteries. Electrochim. Acta. 257, 99–108. doi:10.1016/j.electacta.2017.10.040.

Tsvetkov, M., Zaharieva, J., Milanova, M., 2020. Ferrites, modified with silver nanoparticles, for photocatalytic degradation of malachite green in aqueous solutions. Catal. Today. 357, 453–459. doi:10.1016/j.cattod.2019.07.052.

Uddin, M.K., Baig, U., 2019. Synthesis of Co_3O_4 nanoparticles and their performance towards methyl orange dye removal: characterisation, adsorption and response surface methodology. J. Clean. Prod. 211, 1141–1153. doi:10.1016/j.jclepro.2018.11.232.

Veisi, P., Saeed, M., Dorraji, S., Rasoulifard, M.H., Ghaffari, S., 2021. Synergistic photocatalytic-adsorption removal effect of $NiFe_2O_4$-Zn-Al mixed metal oxide composite under visible-light irradiation. J. Photochem. Photobiol. A Chem. 414, 113268. doi:10.1016/j.jphotochem.2021.113268.

Verma, B., Balomajumder, C., 2020. Synthesis of magnetic nickel ferrites nanocomposites: An advanced remediation of electroplating wastewater. J Taiwan Inst Chem Eng 112, 106–115. https://doi.org/10.1016/j.jtice.2020.07.006.

Wang, A., Zheng, Z., Wang, H., Chen, Y., Luo, C., Liang, D., Hu, B., Qiu, R., Yan, K., 2020. 3D hierarchical H_2-reduced Mn-doped CeO_2 microflowers assembled from nanotubes as a high-performance Fenton-like photocatalyst for tetracycline antibiotics degradation. Appl. Catal. B Environ. 277, 119171. doi:10.1016/j.apcatb.2020.119171.

Wang, Y., Yan, H., Zhang, Q., 2018. Core shell-structured $NiFe_2O_4$@TiO_2 nanoparticle-anchored reduced graphene oxide for rapid degradation of rhodamine B. J Chin Chem Soc 1–7. https://doi.org/10.1002/jccs.201700458.

Wang, Z., Zhang, X., Zhang, H., Zhu, G., Gao, Y., 2019. Synthesis of magnetic nickel ferrite/carbon sphere composite for levofloxacin elimination by activation of persulfate. Sep. Purif. Technol. 215, 528–539. doi:10.1016/j.seppur.2019.01.063.

Wu, S., Shen, L., Lin, Y., Yin, K., Yang, C., 2021. Sulfite-based advanced oxidation and reduction processes for water treatment. Chem. Eng. J. 414, 128872. doi:10.1016/j.cej.2021.128872.

Wu, Y., Shu, R., Li, Z., Guo, C., Zhang, G., Zhang, J., Li, W., 2019. Design and electromagnetic wave absorption properties of reduced graphene oxide/multi-walled carbon nanotubes/nickel ferrite ternary nanocomposites. J. Alloys Compd. 784, 887–896. doi:10.1016/j.jallcom.2019.01.139.

Xiang, B., Ling, D., Lou, H., Gu, H., 2016. 3D hierarchical flower-like nickel ferrite/manganese dioxide toward lead (II) removal from aqueous water. J. Hazard. Mater. doi:10.1016/j.jhazmat.2016.11.011.

Xiao, W., Jiang, X., Liu, X., Zhou, W., Garba, Z.N., Lawan, I., Wang, L., Yuan, Z., 2021. Adsorption of organic dyes from wastewater by metal-doped porous carbon materials. J. Clean. Prod. 284, 124773. doi:10.1016/j.jclepro.2020.124773.

Xiong, Y., Luo, H., Nie, Y., Chen, F., Dai, W., Wang, X., 2019. Synergistic effect of silica coated porous rodlike nickel ferrite and multiwalled carbon nanotube with improved electromagnetic wave absorption performance. J. Alloys Compd. 802, 364–372. doi:10.1016/j.jallcom.2019.06.174.

Xu, J., Li, H., Lowry, G.V., 2021. Sulfidized nanoscale zero-valent iron: tuning the properties of this complex material for efficient groundwater remediation. Account. Mater. Res. 2, 420–431. doi:10.1021/accountsmr.1c00037.

Yan, X., Qian, J., Pei, X., Zhou, L., Ma, R., Zhang, M., 2021. Enhanced photodegradation of doxycycline (DOX) in the sustainable $NiFe_2O_4$/MWCNTs/BiOI system under UV light irradiation. Environ. Res. 199, 111264. doi:10.1016/j.envres.2021.111264.

Yuan, Y., tang Guo, R., fei Hong, L., yin Ji, X., sheng Li, Z., dong Lin, Z., guo Pan, W., 2021. Recent advances and perspectives of MoS_2-based materials for photocatalytic dyes degradation: a review. Colloid. Surface. A Physicochem. Eng. Asp. 611, 125836. doi:10.1016/j.colsurfa.2020.125836.

Zarringhadam, P., Farhadi, S., 2017. Flower-like $Bi_2O_2CO_3$/$NiFe_2O_4$ magnetically recoverable nanocomposites: Preparation, characterization and their catalytic application in the reduction of 4-nitrophenol to 4-aminophenol. J. Alloys Compd. 729, 1046–1057. doi:10.1016/j.jallcom. 2017.09.247.

Zeynizadeh, B., Rahmani, S., 2019. Sulfonyl-bridged (copper-immobilized nickel ferrite) with activated montmorillonite, [($NiFe_2O_4$@Cu)SO_2(MMT)]: a new class of magnetically separable clay nanocomposite systems towards Hantzsch synthesis of coumarin-based 1,4-dihydropyridines. RSC Adv 9, 8002–8015. doi:10.1039/c9ra00177h.

Zhai, L., Bai, Z., Zhu, Y., Wang, B., Luo, W., 2018. Fabrication of chitosan microspheres for efficient adsorption of methyl orange. Chin. J. Chem. Eng. 26, 657–666. doi:10.1016/j.cjche.2017.08.015.

Zhang, Q., Jiang, L., Wang, J., Zhu, Y., Pu, Y., Dai, W., 2020. Photocatalytic degradation of tetracycline antibiotics using three-dimensional network structure perylene diimide supramolecular organic photocatalyst under visible-light irradiation. Appl. Catal. B Environ. 277, 119122. doi:10.1016/j.apcatb.2020.119122.

Zhao, G., Liu, L., Li, J., Liu, Q., 2016. Efficient removal of dye MB: Through the combined action of adsorption and photodegradation from $NiFe_2O_4/Ag_3PO_4$. J. Alloys Compd. 664, 169–174. doi:10.1016/j.jallcom.2016.01.004.

Zheng, Y., Cheng, B., Fan, J., Yu, J., Ho, W., 2021. Review on nickel-based adsorption materials for Congo red. Elsevier B.V. doi:10.1016/j.jhazmat.2020.123559.

Zheng, Y., Cheng, B., You, W., Yu, J., Ho, W., 2019. 3D hierarchical graphene oxide-NiFe LDH composite with enhanced adsorption affinity to Congo red, methyl orange and Cr (VI) ions. J. Hazard. Mater. 369, 214–225. doi:10.1016/j.jhazmat.2019.02.013.

Zhou, Tianhong, Zhang, Guozhen, Zhang, Hongwei, Yang, Hao, Ma, Pengjun, Li, Xiaoting, Qiu, Xiaoli, Liu, Gang, 2018. Highly efficient visible-light-driven photocatalytic degradation of Rhodamine B from a novel Z-scheme Ag_3PO_4/MIL-101/$NiFe_2O_4$ composite. Catalysis Science & Technology 8, 2402–2416. doi:10.1039/C8CY00182K.

Zhu, H., Jiang, R., Fu, Y., Li, R., Yao, J., 2016. Applied Surface Science Novel multifunctional $NiFe_2O_4$/ZnO hybrids for dye removal by adsorption, photocatalysis and magnetic separation. Appl. Surf. Sci. 369, 1–10. doi:10.1016/j.apsusc.2016.02.025.

Ziarati, A., Nadimi, M., Ali, M., 2019. Magnetic $TiO_2/NiFe_2O_4$/reduced graphene oxide nanocomposite as a recyclable photocatalyst for photocatalytic removal of methylene blue under visible light. J. Alloys Compd. 803, 291–306. doi:10.1016/j.jallcom.2019.06.245.